catalysts

MDPI

Review

A Review on Heteroanionic-Based Materials for Photocatalysis Applications

Yathavan Subramanian [1], **Anitha Dhanasekaran** [1], **Lukman Ahmed Omeiza** [1], **Mahendra Rao Somalu** [2] **and Abul K. Azad** [1,*]

[1] Faculty of Integrated Technologies, Universiti Brunei Darussalam, Gadong BE1410, Brunei
[2] Fuel Cell Institute, Universiti Kebangsaan Malaysia (UKM), Bangi 43600, Malaysia
* Correspondence: abul.azad@ubd.edu.bn

Abstract: In the last few decades, photocatalysis has been found to be a practical, environmentally friendly approach for degrading various pollutants into non-toxic products (e.g., H_2O and CO_2) and generating fuels from water using solar light. Mainly, traditional photocatalysts (such as metal oxides, sulfides, and nitrides) have shown a promising role in various photocatalysis reactions. However, it faces many bottlenecks, such as a wider band gap, low light absorption nature, photo-corrosion issues, and quick recombination rates. Due to these, a big question arises of whether these traditional photocatalysts can meet increasing energy demand and degrade emerging pollutants in the future. Currently, researchers view heteroanionic materials as a feasible alternative to conventional photocatalysts for future energy generation and water purification techniques due to their superior light absorption capacity, narrower band gap, and improved photo-corrosion resistance. Therefore, this article summarizes the recent developments in heteroanionic materials, their classifications based on anionic presence, their synthesis techniques, and their role in photocatalysis. In the end, we present a few recommendations for improving the photocatalytic performance of future heteroanionic materials.

Keywords: heteroanionic photocatalysts; photocatalysis; water purification; solar-fuel generation

check for updates

Citation: Subramanian, Y.; Dhanasekaran, A.; Omeiza, L.A.; Somalu, M.R.; Azad, A.K. A Review on Heteroanionic-Based Materials for Photocatalysis Applications. *Catalysts* **2023**, *13*, 173. https://doi.org/10.3390/catal13010173

Academic Editors: Fengxia Deng and Xiaoxiao Zhang

Received: 24 November 2022
Revised: 23 December 2022
Accepted: 30 December 2022
Published: 11 January 2023

1. Introduction

Due to overpopulation, the energy demand and the revolution of industries have increased triple times compared to the 1990s. The depletion of fossil fuels and the harmful effects of industrial pollutants made the world look toward the fabrication of nanomaterials capable of generating energy from greener sources and remediation of contaminants from the environment [1]. In the last few decades, semiconductor-based photocatalysts have shown an excellent capability to decompose organic pollutants from the environment and produce greener fuels, such as hydrogen, hydrogen peroxide, etc., from water using solar radiation [2,3]. The mechanism of semiconductor photocatalysis undergoes the following steps; (i) Light energy of a specific wavelength is allowed to fall onto a material, (ii) If the energy of the incident light is equivalent/higher to the band gap value of the material, it will induce electron excitations from the valence band (VB) to the conduction band (CB) of the material and holes will be left in the VB, (iii) Then the generated charge carriers could undergo subsequent oxidation and reduction reaction with any reactant species, which would be adsorbed on the material surface to provide the necessary intermediate/end products [4,5]. In the beginning stages, traditional photocatalysts such as TiO_2, CdS, Cu_2O, ZnO, etc., have been employed to decompose pollutants and solar-fuel generation such as H_2, H_2O_2, NH_3, etc. Furthermore, it has excellent chemical stability, less fabrication cost, and is non-toxic. However, it faces many bottlenecks, such as a wider band gap, less visible-light absorption nature, photo-corrosion issues, and quick recombination rates [6–13].

Therefore, designing cost-effective and novel visible-light active photocatalysts with enhanced stability and charge separation is much needed. Based on this, researchers believed that adopting homogeneous and heterogeneous structures, polarization field engineering, band gap engineering, etc., will enhance the photocatalyst's stability and recombination rate. Recently, novel structured heteroanionic photocatalysts, such as metal oxynitrides, oxysulfides, oxyhalides, and oxycarbides, have been created based on heteroanionic engineering and begun to show their promising role in the photocatalysis sector [14,15]. Heteroanionic photocatalysts have more than one anion in their structure, which provide enough space for the valence band engineering by careful manipulation of anions [16,17]. Heteroanionic photocatalysts can be prepared with the help of electronic/crystal structure engineering, local coordination geometry, and other techniques [18]. Heteroanionic photocatalysts mainly possess metal cations as the primary elements connected with oxygen and other anion atoms. The VB of these materials is occupied by mixed anion-p and oxygen-2p orbitals. Its conduction band was made up of d^0 or d^{10} orbitals of metal ions; this arrangement induces a narrower band gap with more negative VB than traditional photocatalysts [19,20]. Its band gap structure, good electrical conductivity, and corrosion-resistant characteristics make them more suitable for photocatalysis reactions [21]. Heteroanionic materials are more stable in air/moisture than bare sulfide/oxide/nitrides [22]. Most review articles were primarily reported based on bismuth oxyhalides, tantalum oxynitride, and their applications in photocatalysis [23,24]. However, to the best of our knowledge, a critical review that exclusively focuses on applications of heteroanionic compounds for photocatalysis has not been conducted elsewhere.

Therefore, this review study has been made to provide readers with a comprehensive grasp of the photocatalytic applications of heteroanionic materials, their synthesis procedures, and their advantages over traditional catalysts. Then it summarizes the characteristics of the heteroanionic material, its classification according to the nature of the anions present in them, and its application in photocatalysis. Finally, we present recommendations and outlooks for effectively utilizing and developing various heteroanionic materials to enhance their photocatalysis applications further.

2. Photocatalysis and Its Mechanism

Photocatalysis is a composite word composed of two parts, "photo (light)" and "catalysis". Photocatalysis is a chemical reaction accelerated by light and a substance/semiconductor interaction. [25]. More specifically, when the light of a suitable wavelength is irradiated over a semiconductor, it induces photo-excitation by consuming photon energy. As a result, the electrons from the catalyst VB get excited to the CB by leaving holes in the VB. The energy gap between the VB and CB is known as the "band gap" [26]. It corresponds to the wavelength of the light by which the photocatalyst can effectively absorb it. After photo-excitation, the excited charge carriers would separate and transfer onto the photocatalyst's surface and undergoes subsequent oxidation and reduction reactions with reactant species [27].

During the process of photocatalytic water splitting, the photogenerated electron and hole carriers in the catalyst perform the roles of reducing and oxidizing agents, respectively, to produce hydrogen gas and oxygen gas [28,29]. Figure 1 depicts the mechanism underlying water splitting using photocatalysts in the presence of light.

The photocatalytic splitting of water into H_2 and O_2 is considered an exothermic reaction. It requires a specific Gibbs free energy change of 237 kJ/mol or 1.23 eV to split water molecules successfully, as shown in Equations (1)–(3) [30]. Hence, the band gap of the photocatalyst (E_g) should be at least greater than 1.23 eV to participate in water splitting.

$$\text{Photo-reduction: } 2H_2O + 2e^- \rightarrow H_2 + 2OH^- \tag{1}$$

$$\text{Photo-oxidation: } 2H_2O \rightarrow O_2 + 4H^+ + 4e^- \tag{2}$$

$$\text{Overall reaction: } H_2O \rightarrow H_2 + \frac{1}{2}O_2;\ \Delta G = +237\ \text{kJ/mol} \tag{3}$$

Furthermore, the position of the CB and VB edges of the catalyst is crucial to carrying out both redox reactions of H_2O via photogenerated electron–hole charges. The CB edge of photocatalysts must be more negative than the reduction potential of H^+/H_2 (0 V) vs. standard hydrogen electrode (SHE)). At the same time, the VB should be greater than the oxidation potential of O_2/H_2O.

Similarly, in the photocatalytic degradation of pollutants, photo-induced charge carriers serve as powerful oxidizing and reducing candidates, causing a cascade of subsequent oxidative and reductive processes, as shown in Figure 2.

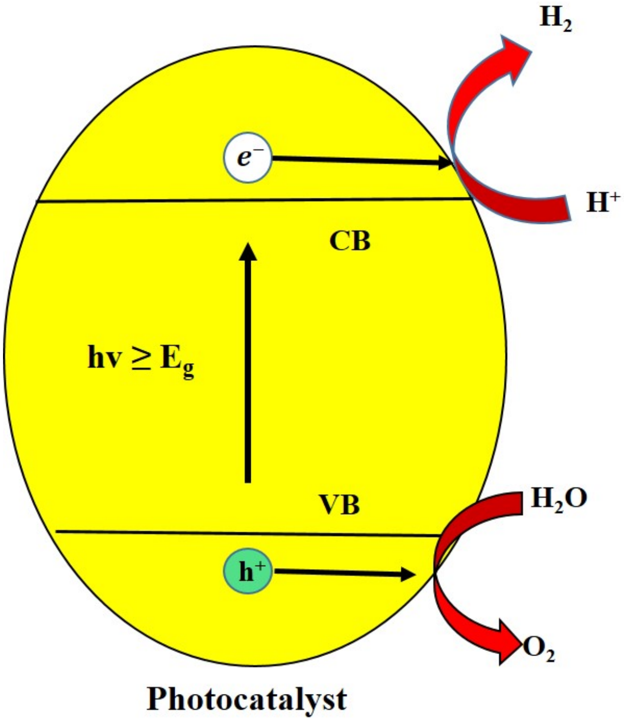

Figure 1. Mechanism of photocatalytic water splitting.

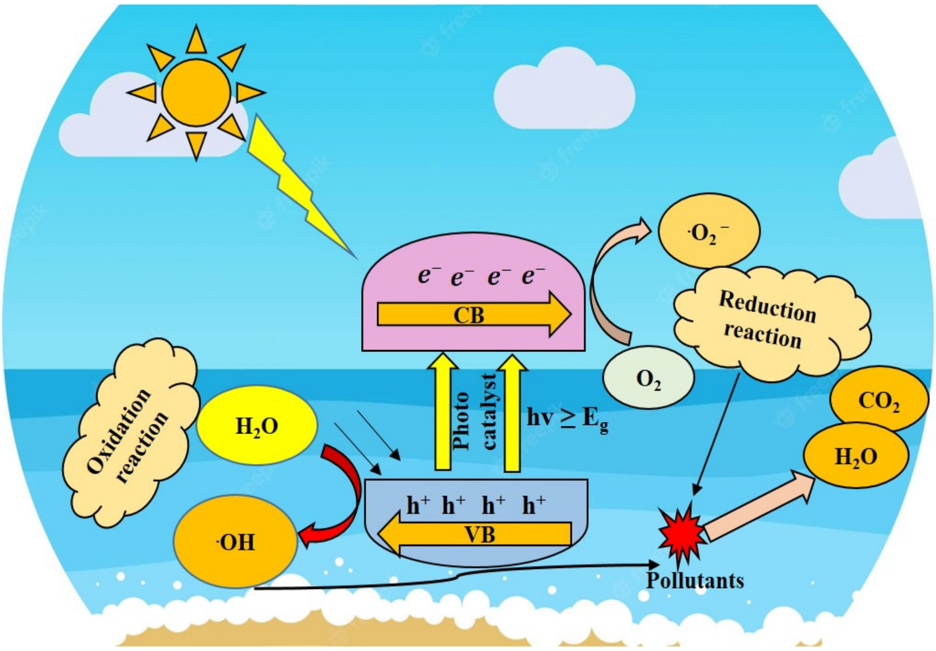

Figure 2. Schematic representation of the mechanism of photocatalytic degradation of pollutants.

The sequence of redox processes involved in photocatalytic pollutant degradation is shown in Equations (4)–(9) [31,32].

$$\text{Photocatalyst} + h\nu \rightarrow e^- + h^+ \quad (4)$$

Photo-oxidation reactions:

$$h^+ + H_2O \rightarrow H^+ + {}^{\cdot}OH \quad (5)$$

$$h^+ + OH^- \rightarrow {}^{\cdot}OH \quad (6)$$

Photoreduction reactions:

$$e^- + O_2 \rightarrow {}^{\cdot}O_2{}^- \quad (7)$$

$$2e^- + O_2 + 2H^+ \rightarrow H_2O_2 \quad (8)$$

$$e^- + H_2O_2 \rightarrow OH^- + {}^{\cdot}OH \quad (9)$$

The formation of hydroxyl and superoxide radicals through redox processes is the principal pathway for photo-induced pollutant degradation, as shown in the general Equations (10) and (11):

$${}^{\cdot}OH^{\cdot} + \text{pollutant} \rightarrow \text{intermediates} + CO_2 + H_2O \text{ (degradation products)} \quad (10)$$

$${}^{\cdot}O_2{}^- + \text{pollutant} \rightarrow \text{intermediates} + CO_2 + H_2O \text{ (degradation products)} \quad (11)$$

In a general photocatalytic degradation process, if the reduction reaction of adsorbed oxygen does not happen simultaneously with pollutant oxidation, there is much possibility for the electrons to gather on the surface of the catalyst, leading to a higher recombination rate of charge carriers. Hence, it is essential to avoid electron accumulation by delivering O_2 molecules into the reaction chamber to achieve a successful photocatalytic process.

3. Advantages and Limitations of Traditional Photocatalysts

In the 1970s, Fujishima and Honda employed titanium dioxide in a photoelectrochemical cell to split water molecules into H_2 and O_2 [7]. Their research also provided the foundation for producing innovative semiconductor photocatalysts to eliminate environmental contaminants and applications in the energy sector [33,34]. Traditional photocatalysts, such as metal oxides, sulfides, nitrides, etc., are utilized in various applications, including hydrogen gas generation through water splitting and water purification via wastewater degradation [35]. Eliminating water contaminants and producing greener fuels through photocatalysis are crucial to meet the rising demand for pure water and energy [36]. Conventional photocatalysts have a wider surface area that aids in purifying polluted water sources and produces greener hydrogen gas without generating environmental damage [37,38]. Traditional photocatalysts can increase the number of active reaction sites on their surface through the interaction of light, resulting in a significant amount of catalytic activity. [39]. Traditional photocatalysts possess distinctive properties, making them a potential candidate for an effective photocatalyst [40,41]. The advantages are outlined below.

- ➢ Conventional catalysts possess promising band gap energy and display enhanced photocatalytic behavior under UV-Visible light [42–44].
- ➢ It enables multi-active areas on their surface to carry out photocatalytic reactions quickly [45].
- ➢ Some photocatalysts have suitable CB and VB edges that are optimal for the reduction and oxidation potentials of H^+/H_2 and O_2/H_2O, respectively [46,47].

Although traditional photocatalysts provide various advantages, they also possess a few disadvantages, as outlined below.

- ➢ Only a few conventional photocatalysts possess a negative CB potential for hydrogen generation. However, many traditional photocatalysts have unfavorable CB edges that are substantially lower than the standard reduction potential, which is essential for hydrogen production by splitting water molecules [48,49].
- ➢ Due to the rapid recombination of electron–hole carriers, the electrons in the CB cannot be successfully tapped by O_2 to form superoxide radicals during the degradation process [50].
- ➢ Some traditional photocatalysts exhibit a lesser surface area reaction with pollutants and less charge-carrier transport, which leads to low pollutant degradation efficiency [51].
- ➢ Although many traditional photocatalysts are paramount, they are not independent [52].
- ➢ Few conventional photocatalysts necessitate an acidic pH between 2.5 to 3.5 for the photo-Fenton reaction [53].
- ➢ Recombination of charge carriers is one of the significant limitations of conventional semiconductor photocatalysts.
- ➢ Few traditional photocatalysts are susceptible to photo corrosion.
- ➢ The reusability of the catalyst is the most critical factor since few materials quickly mix with the reaction chamber when exposed to light radiation [54]. Separating the photocatalyst from the reaction chamber is a difficult task.

Therefore, developing an optimal photocatalyst with the ability to maintain the increase in the density of active reaction sites over a large surface area along with reducing the recombination of charge carriers and the back-reaction rate is much required in recent days. It has motivated considerable research activity over the last few decades and has helped overcome the above limitations by designing heteroanionic materials for photocatalysis applications.

4. Applications of Heteroanionic Photocatalyst in Solar-Induced Direct Pollutant Degradation and Greener Fuel Generation

Heteroanionic engineering is an emerging technique for producing more efficient photocatalysts than conventional photocatalysts. Heteroanionic photocatalysts have more than one anion in their structure [55,56]. Its electrical and thermal properties can be easily adjustable, and its oxidation resistance, chemical inertness, and photon absorption are exceptional [57,58]. It has a smaller band gap than metal oxide complexes because of the lower electronegativity of non-oxide anions in its structure, which facilitates more excellent visible-light absorption [59,60].

Heteroanionic photocatalysts can be classified based on the anionic present in their structure, such as metal oxynitrides (MO_xN_y), oxysulfides ($M_xO_yS_z$), oxyhalides (MOX), oxycarbides (MO_yC_z) [14]. The VB of the heteroanionic photocatalysts is occupied by hybridized anion/oxygen atoms p-orbitals, while its CB is made up of empty d^0 or d^{10} orbitals of metal ions. This configuration induces a smaller band gap with a more negative VB than conventional metal oxides/sulfides/nitrides photocatalysts. These photocatalysts can be synthesized by mixing several anions using various strategies such as electronic/crystal structure engineering and local coordination geometry [61,62]. Heteroanionic photocatalysts produced via in-situ chemical solution procedures have greater efficiencies than those synthesized through physical mixing techniques. Recently, heteroanionic photocatalysts exhibited higher efficiency, principally attributable to the greater separation of electron–hole pairs via interfacial charge transfer and its lower band gap energy. Consequently, the interface between various anions in heteroanionic materials serves as the crucial charge-carrier transfer route during photocatalysis. Due to their stability and high efficiency, these materials have recently created incredible interest in photocatalysis as both catalysts and supports. Figure 3a–e compares the electronic structure of metal oxides with various types of heteroanionic photocatalysts.

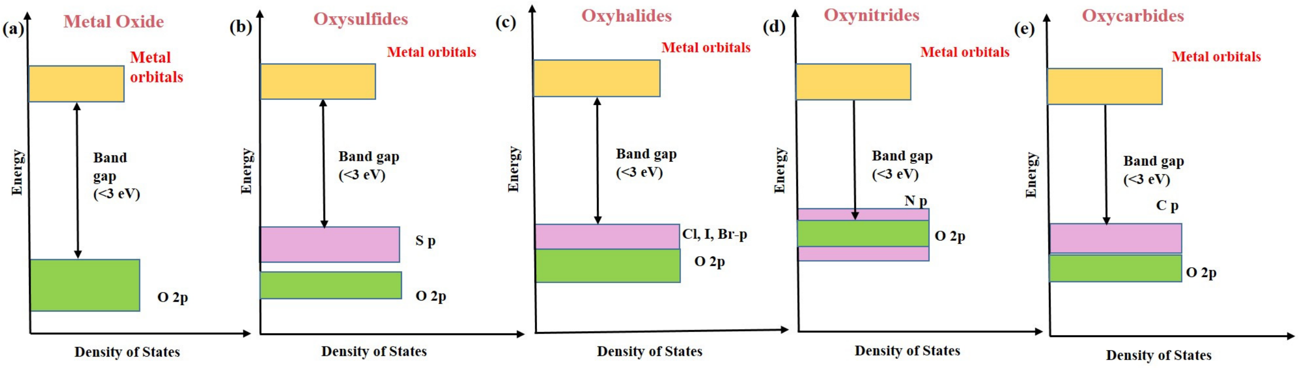

Figure 3. Comparison of the electronic structure of (**a**) metal oxides with (**b**) oxysulfides, (**c**) oxyhalides, (**d**) oxynitrides, and (**e**) oxycarbides photocatalysts [14].

Therefore, this review outlines the few heteroanionic materials classified based on the anion group they contain and highlights their roles in photocatalysis technology.

5. Classification of Heteroanionic Photocatalyst

5.1. Oxynitride-Based Photocatalyst

Metal oxynitrides are one of the emerging photocatalysts that possess combined characteristics of their oxides and nitrides. Oxynitrides photocatalysts mainly have metal cations as the primary element connected with oxygen and nitrogen atoms [63–65]. The VB of these materials is occupied by hybridized N-2p and O-2p orbitals [66,67]. Its conduction band was made up of d^0 or d^{10} orbitals of metal ions; this arrangement induces a smaller band gap with more negative VB than conventional metal oxide/nitride photocatalysts [58,68]. Its band gap structure, good electrical conductivity, and corrosion-resistant characteristics favor photocatalysis. Oxynitrides are more stable in air and moisture than bare nitrides [69]. Pure nitrides are more sensitive to visible and UV light than oxide materials; however, they predominantly suffer from stability issues and cannot maintain their photocatalytic character for a long time. Therefore, researchers attempted to introduce nitrogen into the oxide network to obtain superior physical and chemical characteristics compared to metal oxide and nitride materials. Nitrogen atoms are less electronegative and more polarizable than oxygen atoms, so replacing nitrogen with oxygen helps to narrow down the band gap between the anion-based VB and cation-based CB [70]. Most oxynitrides have suitable band gap values between 1.6–3.3 eV, as necessary for various photocatalytic reactions [62,71]. The following section discusses essential oxynitride-based materials, their synthesis process, and their photocatalytic character.

The synthesis process of oxynitride-based materials is very complex compared to oxide materials. A significant nitriding candidate is needed to prepare oxynitrides photocatalysts from oxide precursors. The most common method for fabricating oxynitrides is thermal ammonolysis [72]. Here, ammonia plays both roles of nitriding (oxidizing) and reducing agent; this dual character is most crucial for the ammonolysis reaction [73]. When the ammonia passes over the oxide precursor, it decomposes over the oxide surface by creating reactive nitriding candidates (N, NH, NH_2) in a native state and H_2 [74]. Then the hydrogen reacts with oxygen atoms from the oxide precursor and escapes as water vapors. This thermodynamic reaction acts as a driving force to introduce nitrogen through the substitution approach, as shown in Equation (12) [75].

$$\text{Oxide} + NH_3\ (g) \rightarrow \text{Oxynitride} + H_2O \tag{12}$$

High pressure is supplied to this process to avoid the decomposition of precursors such as oxides and nitrogen gas. It helps to stabilize the oxynitrides with novel structures at moderate temperatures. Only a few solid-state syntheses of oxynitrides at high pressures have been studied in the literature [76]. The temperature supplied to this process mainly depends upon the choice of the chosen oxide precursor. The purity of the oxynitride phase primarily depends upon the proper control over vital parameters such as temperature, ammonia flow rate, the pressure inside the alumina tube, reaction time, and type of oxide precursor kept inside the alumina tube. Similarly, some oxynitrides have been fabricated in thin films via physical and chemical approaches. For example, thin films of $BaTaO_2N$ have been prepared through pulsed laser deposition [77], and also thin films of $LaTiO_2N$ have been obtained via reactive RF-magnetron sputtering to analyze its photocatalytic performance [78].

In particular, tantalum oxynitride is a promising heteroanionic photocatalyst that possesses suitable valence and conduction band edges to generate H_2 and O_2 from water [79]. It has narrower band gap energy than tantalum oxide [80,81]. As a result, it captures visible light more efficiently and has improved photocatalytic capability. Its crystal structure is monoclinic, where tantalum is hepta-coordinated and interconnected with N and O anions. For instance, Domen et al. explored the photocatalytic characteristics of TaON [82]. It demonstrated a quantum efficiency of 34% for oxygen evolution in the presence of a sacrificial reagent because it has a maximum visible-light absorption capability of up to ~530 nm, with a VB edge of 2.20 eV vs. SHE. It was prepared by heating the Ta_2O_5 on tantalum foil at 1073–1123 K under an ammonia flow of 10 mL min^{-1}. Apart from TaON, most d^0 metal oxynitride belongs to a subgroup named perovskite oxynitrides. Generally, perovskite-structured materials possess promising properties in terms of electric conductivity, light absorption, and high photostability. Perovskite-based oxynitrides (ABO_2N) can be formed by adding nitrogen into the anionic network of the corresponding oxides [83]. It consists of the irregular, corner-shared $BO(N)_6$ octahedra joined by metal cations. It can result in materials with a narrower band gap than the parent oxide. This narrowing happened due to the inclusion of higher energy N-2p orbital along with the O-2p orbital in VB of the parent oxide, making them excellent candidates for visible light-absorbing photocatalysts. The general formula for perovskite oxynitride is termed as $ABO_{2-x}N_{1+x}$ [84]. Ammonolysis is the most common process for producing perovskite-based oxynitrides. Perovskite-type compounds (ABO_2N) are often synthesized by heating the oxide precursors ($A_2B_2O_7$) or mixes of oxides and oxysalts, such as carbonates in the presence of ammonia in the temperature range of 600–1100 °C [73]. Perovskite oxynitrides such as $CaTaO_2N$, $SrTaO_2N$, $LaTaON_2$, and $BaNbO_2N$ oxynitride perovskite also showed promising photocatalytic characteristics [85]. Their band gap and edge positions offered significant activity over water oxidation and reduction processes. The general crystal and band gap structure of a few perovskite oxynitrides are shown in Figure 4a,b [86].

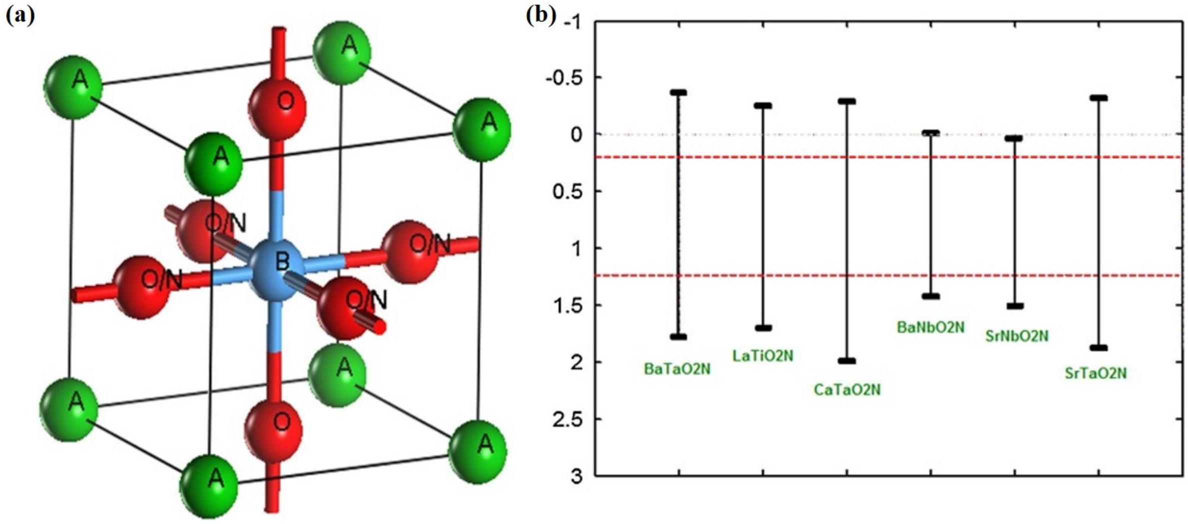

Figure 4. (**a**) Crystal structure of perovskite oxynitride; (**b**) band gap structure of perovskite oxynitrides. Reproduced with permission [86], Copyright 2016, Elsevier.

Perovskite oxynitrides possess a narrower band gap value of 1.5−2.5 eV than TiO_2 and are more stable under various reaction mediums [87]. It also has favourable CB and VB edges for photocatalytic water splitting [88]. For example, the band gap and crystal structure of $BaTaO_2N$ are shown in Figure 5a. In addition, the UV-visible absorption spectra for some perovskite (oxy) nitrides are demonstrated in Figure 5b [58].

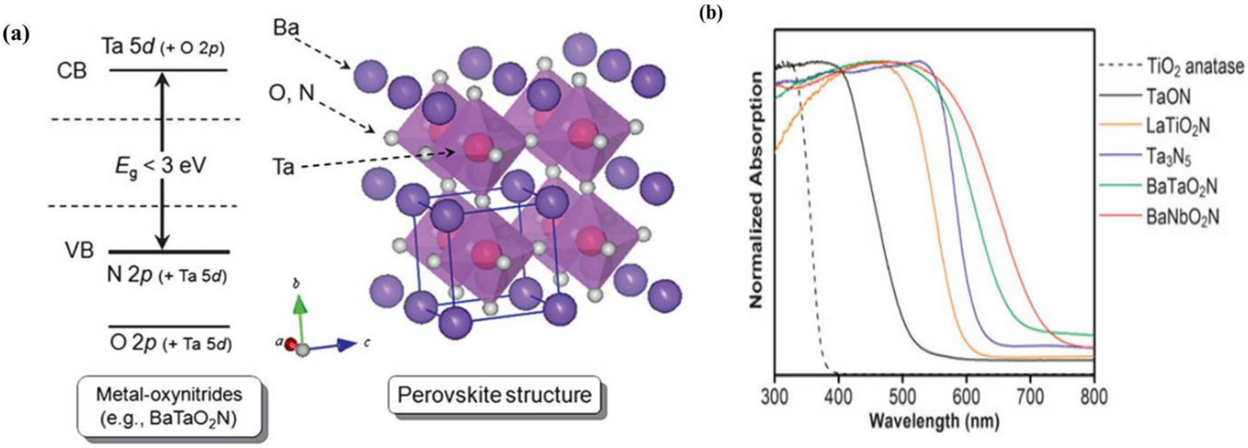

Figure 5. (**a**) Crystal structure of perovskite oxynitride $BaTaO_2N$ photocatalyst; (**b**) absorption spectra of few important oxynitrides. Reproduced with permission [58], Copyright 2011, Springer Nature.

In 2002, the first study on water splitting into hydrogen and oxygen using a perovskite-based oxynitride was published. Kasahara et al. synthesized $LaTiO_2N$ through thermal ammonolysis and reported its promising H_2 and O_2 generation activity in the presence of the sacrificial reagents [89]. Moreover, Shunhang Wei studied the influence of adding the extra layer of SrO in the $SrTaO_2N$ materials by forming Sr_2TaO_3N because the Sr_2TaO_2N photocatalyst undergoes self-oxidative decomposition even in the presence of hole scavenger protection. The crystal structure of the Sr_2TaO_3N and $SrTaO_2N$ can be seen in Figure 6a. From the absorption graph of Figure 6b, it is found that the inclusion of an extra layer of SrO significantly increased the light absorption character of Sr_2TaO_3N compared to $SrTaO_2N$, and it possesses more excellent photostability. During the oxygen evolution process, Sr_2TaO_3N supported with the CoOx co-catalyst performed better than the $SrTaO_2N$, as is shown in Figure 6c,d [90].

Furthermore, $BaNbO_2N$, a niobium-based oxynitride, was prepared by Hisatomi and their team by nitriding the $Ba_5Nb_4O_{15}$ (oxide precursor) under an NH_3 gas. It absorbs more light up to 740 nm, one of the longest wavelengths ever observed for an oxynitride photocatalyst. They also determined its water-splitting behavior can be increased in the presence of sacrificial reagents and by loading suitable co-catalysts [91–93].

Harshavardhan Mohan et al. produced nickel-coated manganese oxynitride/graphene sheets to increase the base materials' surface area and band gap energy value. The band gap value of the manganese oxide reduced from 2.10 eV to 1.97 eV due to the addition of nitrogen and nickel in the MnO structure. The composite demonstrated a high degradation activity over acetylsalicylic acid under visible-light illumination and had good structural stability even after being used multiple times [94].

The results of the above-reported investigations demonstrated that metal oxynitride could be made more robust through the surface and interface modification. These modifications enhance the durability of metal oxynitride by regulating h^+ extraction and driving them to realize as visible-light absorption catalysts. Future developments that strengthen the endurance of metal oxynitrides may be achievable by understanding how durability can be engineered in future heteroanionic materials. The photocatalytic (H_2 and O_2 generation) activity of a few essential oxynitrides is detailed in Table 1.

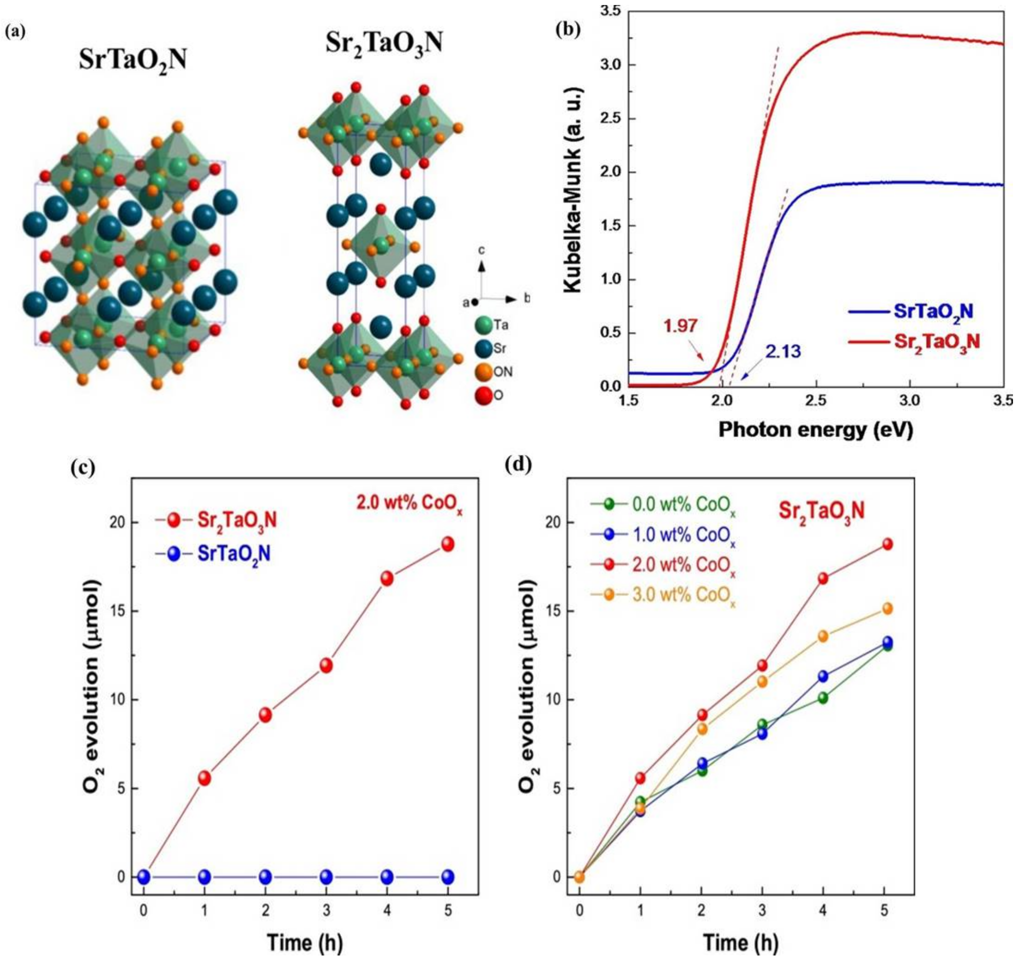

Figure 6. (**a**) Atomic arrangement of the Sr_2TaO_3N and Sr_2TaO_2N photocatalyst; (**b**) band gap energy of both photocatalyst; (**c**) oxygen evolution rate of $SrTaO_2N$ and Sr_2TaO_3N when loaded with 2.0 wt% CoO_x under visible light; (**d**) oxygen evolution rate of Sr_2TaO_3N with various percentage of CoO_x co-catalyst in the presence of $AgNO_3$. Reproduced with permission, [90] Copyright 2018, Elsevier.

Table 1. List of few reported oxynitride photocatalysts, their crystal structure, band gap, and amount of H_2 and O_2 evolved.

S. No	Name of the Photocatalyst	Crystal Structure	Band Gap Value (eV)	Amount of H_2 Gas Evolved	Amount of O_2 Gas Evolved	Reference
1	$CaNbO_2N$	Perovskite	1.9	1.5 μmol h^{-1}	46 μmol h^{-1}	[95]
2	$LaTiO_2N$	Perovskite	2.0	30 μmol h^{-1}	41 μmol h^{-1}	[95]
3	$CaTaO_2N$	Perovskite	2.5	15 μmol h^{-1}	0	[88]
4	$SrTaO_2N$	Perovskite	2.1	20 μmol h^{-1}	0	[88]
5	$BaTaO_2N$	Perovskite	2.0	15 μmol h^{-1}	0	[88]
6	$LaTaON_2$	Perovskite	2.0	20 μmol h^{-1}	0	[95]
7	TaON	Baddelyite	2.5	15 μmol h^{-1}	660 μmol h^{-1}	[95]
8	$SrTaO_3N/CoO_X$	Perovskite	1.97	0	20 μmol	[90]
9	GaON	Wurtzite	2.2 to 2.8	18 μmol h^{-1}	30 μmol h^{-1}	[96]
10	ZnO:InN oxynitride	Wurtzite	2.82	48 μmol/g	0	[97]

5.2. Oxyhalide-Based Photocatalyst

Metal oxyhalides (MOX) have played a potential role in solar–fuel generation and water purification processes due to their promising energy band gap structure and light absorption properties [98,99]. These characteristics mainly depend upon the type of halide engineered in its structure. Bismuth oxyhalides - BiOX (X = Cl-3p, Br-4p, I-5p) are the most commonly employed heteroanionic catalysts due to their easy band gap tuning nature [100,101]. The visible-light absorption character of BiOX dramatically depends upon the size of the halogen ion. If the size of the halogen increases, its polarizability character also increases from Cl to I. These compounds are composed of $[Bi_2O_2]^{+2}$ layers between double slabs of halogen atoms [102,103]. Their crystal structure is shown in Figure 7a–c [104].

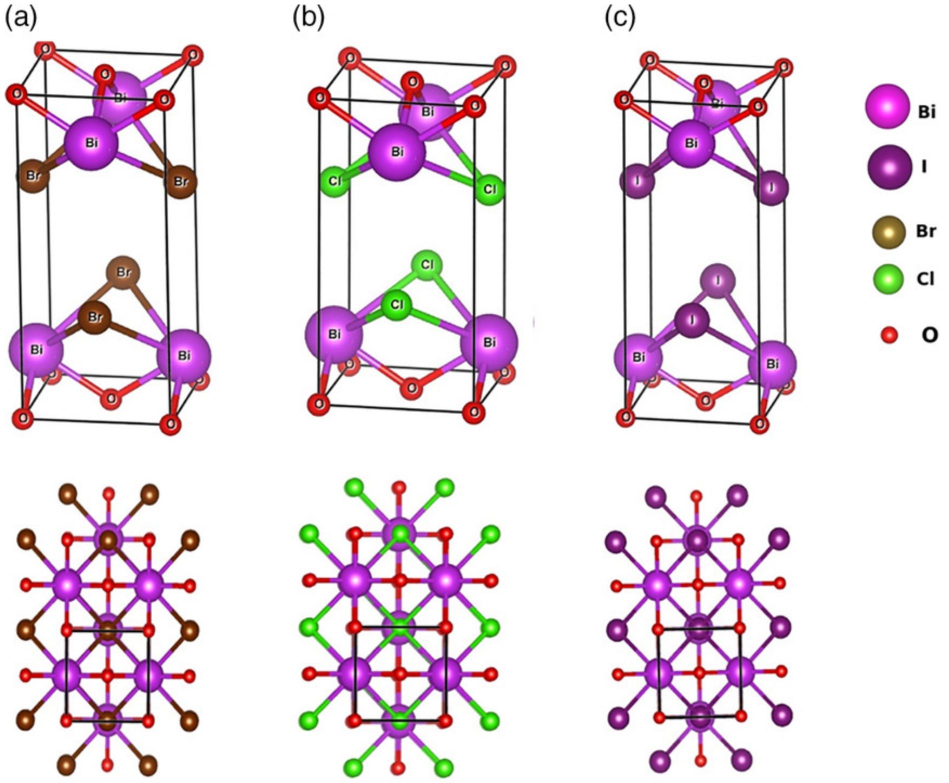

Figure 7. Crystal structure of (**a**) BiOBr, (**b**), BiOCl, and (**c**) BiOI photocatalysts. Reproduced with permission [104], Copyright 2020, Elsevier.

This kind of arrangement induces an internal electric field within the BiOX structure. The internally generated electric field improves the lifetime of photogenerated electron–hole pairs and reduces the recombination rate when irradiated by the light of appropriate energy [105,106]. BiOX-based photocatalysts show some favorable characteristics, such as chemically stable, non-toxic, and anti-corrosive nature [107]. Furthermore, BiOX materials are more sensitive and responsive to visible light than UV light due to their narrower band gap [108]. The VB maxima of BiOX compounds are comprised of O-2p and X-p orbitals, whereas their CB maxima consist of Bi-6p orbitals [109–111]. BiOCl has a wider band gap value of 3.2 eV and demonstrates a significant photocatalytic character under UV light [112]. Similarly, BiOBr (2.64 eV) has a suitable band gap and redox potential, which encourages the conversion of the oxygen molecule into O_2^- radicals and H_2 into H^+ ions [113,114]. However, BiOI is very complex to attain the redox potential due to its narrow band gap value of 1.77 eV [108,115].

The most common techniques for producing BiOX are hydrothermal [116], calcination [117], precipitation [118], microwave [119], reverse micro-emulsion [120], sonochemical methods [121], and template approaches [122]. These approaches helped to enhance visible-light absorption and photocatalytic character. The band gap structure of a few essential oxyhalide photocatalysts is shown in Figure 8 [123].

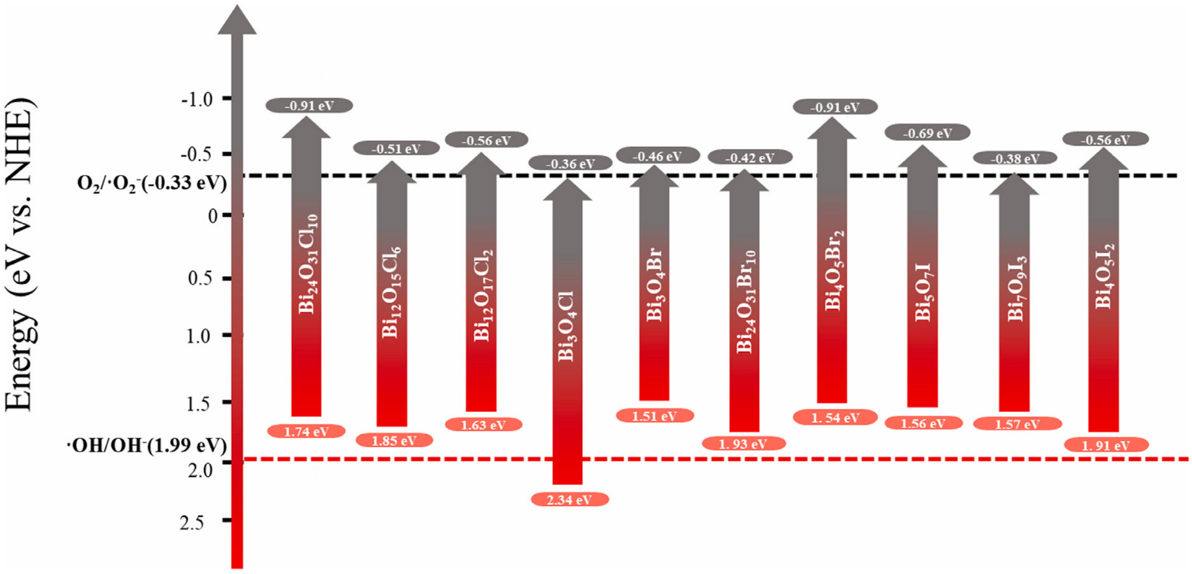

Figure 8. Band gap structure of few important oxyhalide photocatalysts. Reproduced with permission [123], Copyright 2021, Elsevier.

Mainly, Yu and Han et al. analyzed the influence of the solvent used for the fabrication process on the band gap structure and morphology of BiOCl, BiOBr, and BiOI photocatalysts. They used different solvents such as water, acetic acid, N, N-dimethylformamide, glycerol, ethylene glycol, and ethanol to prepare BiOX [124]. Figure 9 a–d shows that the surface morphology of prepared BiOX compounds changes while using different solvents in the preparation process. Then the synthesized BiOX samples were utilized to degrade various pollutants such as tetracycline, rhodamine B, and methyl orange. They found that pure BiOCl and BiOBr, produced using ethylene glycol, had a more photocatalytic activity with respect to tetracycline and rhodamine B than BiOI, as shown in Figure 9e,f. However, in the case of the degradation of methyl orange, BiOI responded well compared to BiOCl and BiOBr (Figure 9g–i) [124].

Even though pure BiOX has demonstrated good photocatalytic activity in removing organic pollutants, it still faces problems, such as the low usage of the solar spectrum and the high recombination rate of charge carriers. Therefore, researchers attempted to solve these bottlenecks by doping metal/nonmetal ions and forming BiOX composites. For instance, Jei Cui and their colleagues produced Ni-BiOCl via a one-step solvothermal process to analyze its degradation behavior over Rhodamine B [125]. Ni-BiOCl photocatalysts decomposed Rhodamine B within 5 min under visible–light irradiation and performed better than the bare BiOCl. These studies confirmed that the doping of foreign ions could significantly improve the photocatalytic efficiency of MOX materials by tuning and enhancing their band gap energy and surface area reaction sites, respectively. Xia and their team also designed BiOCl and BiOBr-based photocatalysts by combining them with carbon quantum dots [126]. The weight percentage of carbon quantum dots and the type of halide present in the composites decide the performance of the photocatalytic activity. They found that BiOBr-based composites with 3 wt% carbon quantum dots effectively remove bisphenol A, phenol, and rhodamine B from the aqueous solution. BiOBr/carbon quantum dots show good optical absorption and an improved charge separation rate, effectively improved by carbon quantum dots. Numerous studies on BiOX-based composites, such as Fe_3O_4/BiOI [127], BiOX/TiO_2 [128], etc., have been conducted. In addition, attempts have been made to develop BiOX-based ternary composite, such as Cd/CdS/BiOCl [129], Ag/AgCl/BiOCl [130], etc., to evaluate their photocatalytic activity.

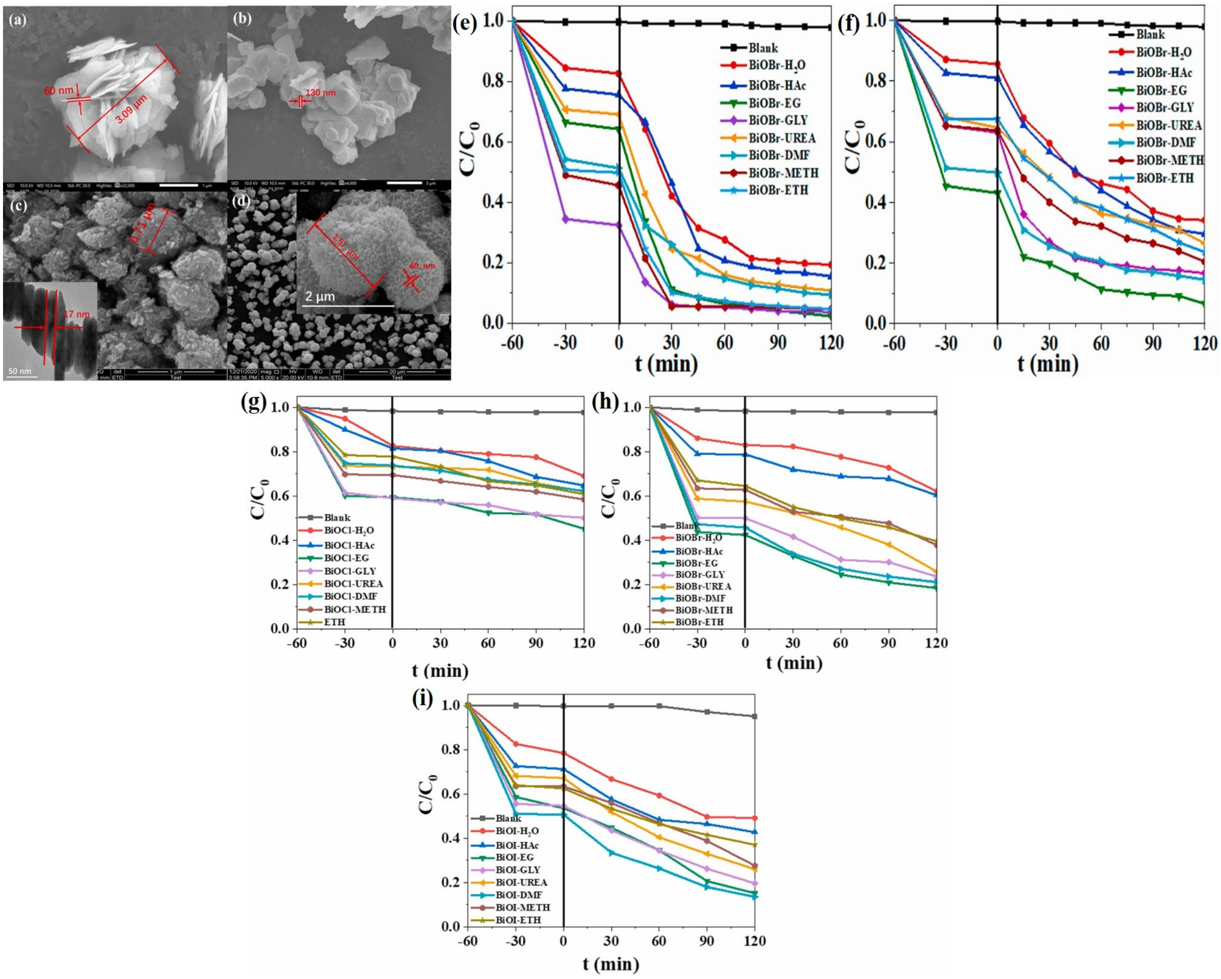

Figure 9. SEM graphs of (**a**) BiOBr, (**b**) BiOI synthesized using water, (**c**) BiOBr, (**d**) BiOI prepared using ethylene glycol, (**e**) photocatalytic behavior of BiOBr over tetracycline in the presence of simulated sunlight, (**f**) under visible light; (**g**) photocatalytic behavior of BiOCl (**h**) BiOBr and (**i**) BiOI over methyl orange dye under visible light. Reproduced with permission [124], Copyright 2021, Elsevier.

BiOX-based materials also played a dominant role in hydrogen generation via photocatalytic water splitting. For instance, Gang-Juan Lee et al. produced flower-like BiOX catalysts using a solvothermal technique with microwave assistance [131]. BiOI generated a maximum H_2 evolution rate of 1316.9 mol $h^{-1}.g^{-1}$ in 360 min at a pH value of 7; this was the highest of all the compounds. BiOI has a small band gap value and suitable conduction band edges, which is sufficient for H_2 generation and has the better capability to separate the photogenerated electrons and holes. Zhidong Wei et al. also synthesized a new type of photocatalyst, such as Bi_4MO_8X (M = Nb, Ta; X = Cl, Br), via a solid-state reaction method [132]. They studied how adding a sacrificial reagent to a photocatalyst enhanced its H_2 generation performance. When glycerol was used as a sacrificial reagent, Bi_4NbO_8Br was found to have superior hydrogen generation performance than all other samples due to its large amount of α-OH and lower standard oxidation potentials. In the last few decades, $Bi_xO_yX_z$ also exhibited promising photoreduction of carbon dioxide to solar fuel (CH_3OH, CH_4, CO, etc.) compared to its capacity to split water molecules into hydrogen. For instance, microspheres of $Bi_4O_5Br_2$ were produced through the glycerol precursor route (Figure 10a) and utilized for the photoreduction of CO_2. The prepared $Bi_4O_5Br_2$ could significantly reduce CO_2 into solar fuels (CH_4 = 2.04 and CO = 2.73 mmol g^{-1} h^{-1}) under sunlight due to its bismuth-rich and ultrathin structure. It is higher than that of ultrathin BiOBr (CH_4 = 0.16 and CO = 2.67 mmol g^{-1} h^{-1}) and bulk BiOBr (CH_4 = 0.16 and CO = 2.67 mmol g^{-1} h^{-1}), as shown in Figure 10b–d [133]. In addition, new oxyhalides such as $Bi_4O_5I_2$, Bi_4O_5BrI, $Bi_4O_5Br_2$, and Bi_5O_7I were also created to assess their photoreduction behavior over CO_2 to produce solar fuels [134].

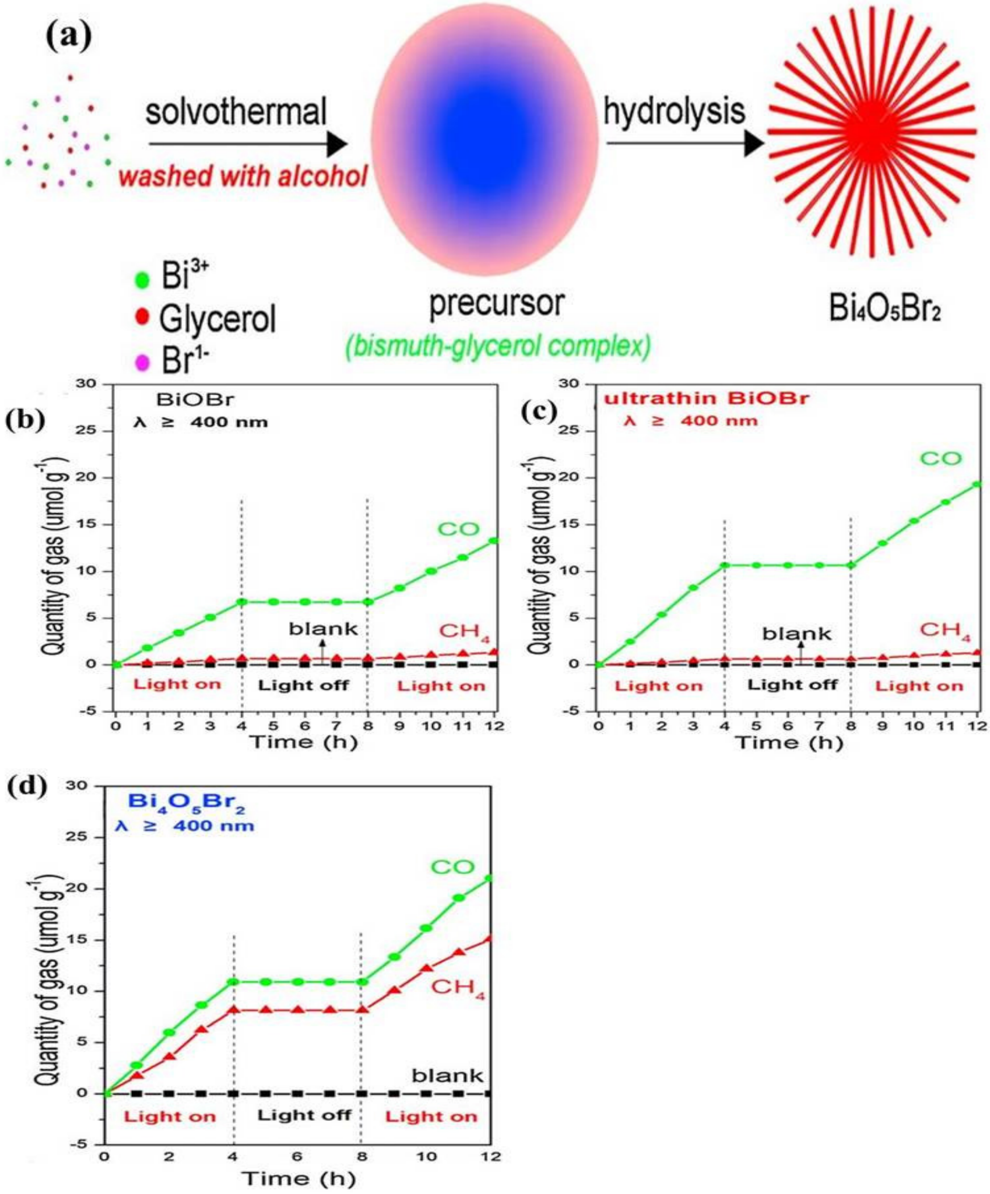

Figure 10. (**a**) Preparation process of $Bi_4O_5Br_2$ using glycerol precursor route, photocatalytic CO_2 reduction activity of (**b**) BiOBr, (**c**) ultrathin BiOBr, and (**d**) $Bi_4O_5Br_2$. Reproduced with permission [133], Copyright 2016, Elsevier.

Oxyhalide photocatalyst also reported promising characteristics in the case of the photocatalytic nitrogen fixation process. In particular, Li et al. first reported nitrogen fixation using the BiOCl photocatalyst in 2015 [135]. Moreover, Li and their team proved that the nitrogen fixation rate (12.72 mmol g^{-1} h^{-1}) of oxyhalides (Bi_5O_7Br) could be improved by increasing oxygen vacancy concentration [136]. In another work, Lan et al. determined the influence of oxygen vacancies in BiOI on photocatalytic nitrogen fixation [137]. They prepared hydrogenated Bi_5O_7I (H-Bi_5O_7I) by annealing in a hydrogen atmosphere at 300 °C for 4 h, and also bare Bi_5O_7I was used for comparison. Electromagnetic resonance signals have found that H-Bi_5O_7I has more oxygen vacancy concentration than the bare Bi_5O_7I due to hydrogenation. This is presumably due to a high number of oxygen atoms detaching from the surface of Bi_5O_7I during hydrogenation. Even in photocatalytic nitrogen fixation studies, H-Bi_5O_7I produced a good amount of ammonia after 180 min of light illumination at a rate of 162.48 mol g^{-1} h^{-1}. It also found that the quantity of ammonia produced rose approximately linearly with the illumination period. This performance was significantly superior than the pure Bi_5O_7I, indicating that oxygen vacancies play an essential role in the adsorption and activation of nitrogen molecules.

Based on the available reports, it has been found that most of the MOX catalysts were synthesized through more time and energy-consuming processes such as solvothermal and hydrothermal. Hence, future research must concentrate on simple and less time-consuming approaches to produce oxyhalide materials. For instance, the microwave-assisted method enables the quick manufacture of oxyhalide materials; however, research into this technique is still in the beginning stage. In addition to surface modification, investigating catalytic processes on the atomic level during various photocatalysis processes is most required because the active sites in the catalysts play a crucial role during reactions. More in situ characterization must be done on oxyhalide materials to understand the keen relationship between the catalyst reaction sites and their catalytic efficiency. Furthermore, most research reports on oxyhalide materials were based only on BiOX-based photocatalysts. Hence, it is necessary to fabricate a new type of oxyhalide-based photocatalysts (such as NbOCl, $VOCl_3$, etc.) to employ them in the degradation process of environmental pollutants and solar-fuel generation and make them more accessible in the future. Table 2 summarizes the different forms of oxyhalide and their applications in various solar-induced catalytic reactions.

Table 2. Summarization of studies on various oxyhalide-based materials for solar-induced different photocatalytic reactions.

S. No	Name of the Photocatalyst	Band Gap Value (eV)	Name of Pollutant	Degradation Efficiency/Evolution Rate	Light Illumination Time	Reference
1	BiOCl	3.43	Rhodamine B	100%	60 min	[138]
2	$BiOIO_3$	3.10	Heavy metal mercury	76%	12 h	[139]
3	Bi_5O_7I nanosheets/nanorods	3.06 eV (Nanorods) and 3.09 eV (nanosheets)	Heavy metal mercury	33% (nanorods) 52% (nanosheets)	70 min	[140]
4	Ce-doped BiOBr	2.87	RhB	99.22%	40 min	[141]
5	Co–Bi_3O_4Br	2.21	CO_2 reduction to CO	2142.1 µmol g^{-1}	20 h	[142]
6	BiOCl-OV-rich	3.12	O_2 evolution	344 µmol g^{-1} h^{-1}	5 h	[143]
7	BiOBr-OV	2.8	N_2 photofixation	104.2 µmol h^{-1}	60 min	[135]
8	BiOCl-OV	3.33	CO_2 reduction to CO	35.03 µmol g^{-1}	4 h	[112]
9	Cobalt doped BiOCl ultrathin nanosheets	2.96	Carbamazepine	86.4%	180 min	[144]
10	Sr-BiOI	1.73	Indomethacin	98%	60 min	[145]
11	Defect-rich single unit cell Bi_3O_4Br	2.29	Photocatalytic reduction of nitrogen	25.4 µmol L^{-1}	1 h	[146]
12	Bi_4SbO_8Cl	2.53	Hydrogen generation	120 µmol	200 min	[147]
13	$Bi_4O_5I_2/Bi_4O_5I_2$	1.89	Degradation of RhB	98%	90 min	[148]

5.3. *Oxysulfide-Based Photocatalyst*

Oxysulfide photocatalyst has a chemical composition between the oxide and chalcogen photocatalysts [149]. It possesses at least a metal, oxygen, and sulfur in its crystal structure with negative oxidation states for both O and S [150]. It is an independent group from metal oxide and metal sulfide. It can be coined with the generic formula $M_xO_yS_z$. Their VB is composed of the sulfur and oxygen orbitals, and d^0/d^{10}-metal ion orbitals occupy the conduction band (e.g., $SrZn_2S_2O$, $Ln_2Ti_2S_2O_5$, etc.) [151]. It possesses narrower bandgaps that are more favorable for photocatalytic water splitting under visible-light exposure due to its sulfide ions, which shift its valence band edges to the negative potential. Most oxysulfide is not available in nature; it needs to be synthesized. In 1947, Pitha and their team fabricated the first crystalline oxysulfide called La_2O_2S [152], and in 1949, Zachariasen synthesized some La_2O_2S, Ce_2O_2S, and Pu_2O_2S [153]. For instance, La_2O_2S can be made by reducing $Ln_2(SO_4)_3$ using hydrogen gas or heating the Ln_2S_3 in the presence of air. It has been found that La_2O_2S is made up of one metal atom that was interconnected with four atoms of oxygen and three atoms of sulfur with a space group of P-3m1. Most metal oxysulfides are fabricated by treating the oxide precursors with sulfur/metal sulfide. However, the band gap tuning of oxysulfide is very complex by varying stoichiometric ratios because sulfur has larger atomic radii than oxygen.

Metal sulfides such as CdS and ZnS generally show excellent absorption in visible light. It has the capacity to generate a considerable amount of H_2 through the photoreduction of H+ ions with the support of the electron donors such as S^{2-} and ${SO_3}^{2-}$. The significant bottlenecks of metal sulfide are subjected to photo-corrsion, because S^{2-} anions are sensitive to oxidation by photogenerated holes [154]. These drawbacks can be rectified by synthesizing more stable oxysulfide compounds [155]. For instance, Wang and their team prepared $Y_2Ti_2O_5S_2$ through a solid-state reaction with tetragonal symmetry [16]. It possesses a narrower band gap energy of 1.9 eV, which absorbs a massive region of solar radiation even up to the wavelength of 650 nm. The conduction and valence band maximum of prepared $Y_2Ti_2O_5S_2$ lies between 1.1 to -1.0 V and 0.8–0.9 V versus SHE, respectively. It has been found that Ti-3d orbitals occupy their CBM, whereas VBM is mixed up with O-2p, S-3p, and Y-3d orbitals. Their band edge positions favored H_2 and O_2 generation via photocatalytic water splitting. These photocatalysts produced considerable hydrogen and oxygen gas when supported with IrO_2 and Rh/Cr_2O_3 during the oxygen and hydrogen evolution process by maintaining pH values around 8–9. During the photocatalysis study, it was found that $Y_2Ti_2O_5S_2$ has more chemical and photostability. Their experiment results are shown in Figure 11a–e [16].

Similarly, Ishikawa and their team prepared $Sm_2Ti_2O_5S_2$ oxysulfide-based photocatalysts with a band gap value of 2.0 eV [149]. It possesses a suitable conduction band edge position, which acts as a driving force for photocatalytic water splitting. In the case of pollutant degradation, oxysulfide photocatalysts also served as promising candidates. Hairus Abdullah and their team recently used indium oxysulfide for hexavalent chromium detoxification [156]. Indium oxysulfide was prepared through a solution-based reaction between indium chloride and thioacetamide at 90 °C. It showed an excellent degradation behavior of Cr(VI) within 15 min without employing any hole scavengers due to its narrower band energy of 2.4 eV. Then it also combined with Ag to test its performance for photocatalytic water splitting. It generated nearly 400 mol/g of hydrogen gas in ethanol solution under exposure to 150 W Xe-lamp irradiation for 5 h. Ma and their group also used $La_5Ti_2CuS_5O_7$-based heteroanionic materials to act as photocathodes/anodes to analyze their behavior in the water-splitting process [157]. Then Hisatomi et al. prepared a novel $La_5Ti_2Cu_{1-x}Ag_xS_5O_7$ and investigated its potential in the H_2 evolution process through the photoelectrochemical cell [158]. Kiyonori Ogisu et al. prepared Lanthanum–Indium oxysulfide to boost the reduction reaction of H+ to molecular hydrogen and oxidize water molecules to oxygen under light illumination in the presence of a sacrificial agent [159]. It possesses a band gap energy of 2.60 eV and acceptable reduction and oxidation potentials for oxygen and hydrogen evolution reactions in the presence of IrO_2 and Pt, respectively, as co-catalysts.

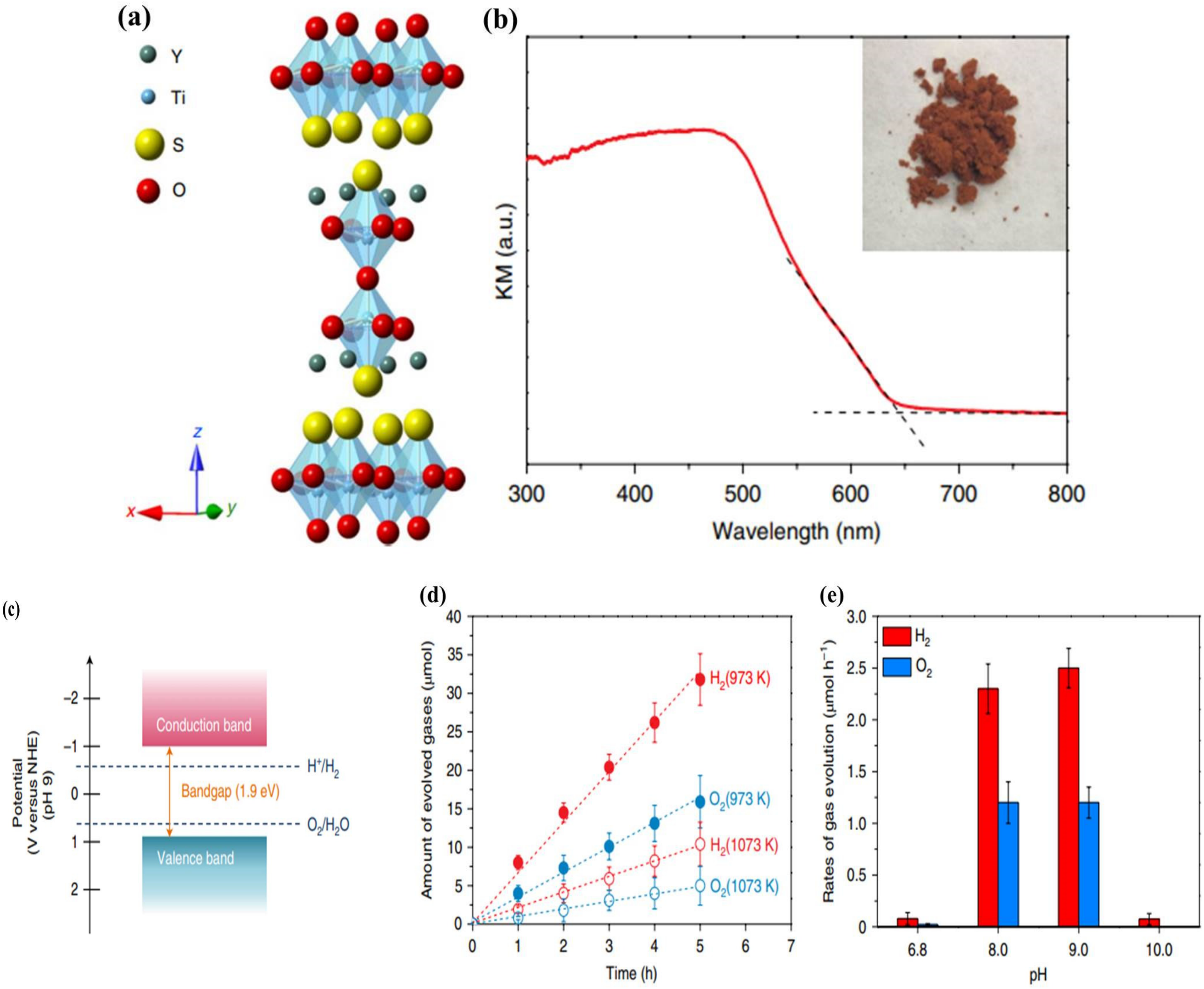

Figure 11. (**a**) Crystal structure of $Y_2Ti_2O_5S_2$ photocatalyst; (**b**) diffuse reflectance spectra for $Y_2Ti_2O_5S_2$; (**c**) band gap structure of $Y_2Ti_2O_5S_2$ (**d**) represents the amount of hydrogen and oxygen gas produced by Cr_2O_3/Rh/IrO_2-modified $Y_2Ti_2O_5S_2$ prepared at two different temperatures in the presence of La_2O_3 (pH 8.5); and (**e**) gas evolution rates of Cr_2O_3/Rh/IrO_2-modified $Y_2Ti_2O_5S_2$ at various pH. Adapted with permission from ref. [16], Copyright 2019, Springer Nature.

Xin-de tang et al. mainly adopted a new approach to prepare a $La_3NbS_2O_5$ photocatalyst [160]. They prepared different types of $La_3NbS_2O_5$ samples by varying the sulfurization time (0.5, 1, and 2 h) and temperatures (1023, 1073, 1123, 1173 K) supplied to it and compared them with $La_3NbS_2O_5$ prepared through solid-state reaction. This study significantly reduced the time required to prepare $La_3NbS_2O_5$ to 1.0 h compared to the traditional solid-state approach (9 days). The band gap energy of $La_3NbS_2O_5$ (2.13−2.17 eV) prepared via the sulfurization process was found to be a little narrower than the $La_3NbS_2O_5$ samples prepared through solid-state reaction (2.26 eV). The maximum H_2 evolution activity was seen for the sample prepared at 1073 K for 1 h, which was approximately 1.83 times that of $La_3NbS_2O_5$ generated by the solid-state reaction. Table 3 summarizes the few photocatalytic studies on oxysulfide photocatalysts.

Table 3. List of oxysulphide-based photocatalysts with their band gaps and H_2 evolution in different experiments.

S. No	Name of the Photocatalyst	Band Gap Value (eV)	Amount of H_2 Gas Evolved	Reference
1	Pt-$SrZn_2S_2O$	3.9	67.8 µmol	[150]
2	Ag-InOS	2.4	400 mol/g	[156]
3	Pt–$LaInS_2O$	2.6	9 µmol h^{-1}	[159]
4	Rh/Ag–$Sm_2Ti_2S_2O_5$	2.1	949 µmol h^{-1}	[161]
5	Pt–$La_5Ti_2AgS_5O_7$	1.5	225 µmol h^{-1}	[162]
6	Pt–La_3GaS_5O	2.3	108 µmol h^{-1}	[163]
7	Cr-TPPCl dye modified n-Bi_2O_2S/In_2O_3 (with Co_3O_4)	1.5	75.1 µmol	[164]

In conclusion, research on oxysulfide catalysts is significantly less than other heteroanionic materials. Therefore, it is necessary to develop new oxysulfide compounds to increase their catalytic studies because sulfide-based materials generally possess promising characteristics. Furthermore, attempts such as surface modification should be made on the oxysulfide materials to improve their catalytic efficiency via loading suitable co-catalysts (apart from pt), ion doping, coupling with carbon materials, hetero-junction engineering, etc. It helps to extract h^+/e^- from oxysulfide and induce a strong hybridization between S- and O-orbitals near the VBM.

5.4. Oxycarbide-Based Photocatalyst

Oxycarbide-based materials are among the newest photocatalysts; they contain a metal ion linked to oxygen and carbon atoms. [165]. Their electrical and thermal properties are easily modifiable, and their oxidation resistance, chemical inertness, and photon absorption are exceptional. They exhibit a small band gap structure. The VB of these materials is occupied by mixed C-2p and O-2p orbitals, while its CB is composed of empty d orbitals of metal ions [19,20]. This configuration induces a smaller band gap with a more negative VB than conventional metal oxide photocatalysts [166]. It can be obtained by regulating the calcination temperature and environment in a complex manner during the synthesis process. Due to their stability and high capacity, most oxycarbide-based compounds were utilized as anodes in the batteries [167–169]. Compared to typical photocatalysts, their preparation procedures are pretty tricky. Moreover, a strong interface between various anions in oxycarbide plays a significant role in photocatalytic degradation by enhancing its charge-carrier transfer route.

For instance, Kan Huang and their team produced highly conductive titanium oxycarbide by reducing titanium oxide in a carbothermic environment [170]. Titanium dioxide was thermally coated with carbon by heating 10% acetylene in N_2 at 700 degrees Celsius for 20 min in a quartz tube furnace. After applying the carbon coating, their products are calcined at 900 and 1100 °C for four hours in an H_2/N_2 mixture. They observed that titanium oxycarbide exhibited significant photocatalytic activity in oxygen evolution reactions. Also, platinum-coated titanium oxycarbide was more effective in ORR and OER processes. Then, Sujun Guan and their colleagues found that the heat treatment of titania coatings in a carbon environment increases their photocatalytic activity. They produced two titania coatings by mechanically coating titanium powder over alumina balls at 480 rpm for 10 h. Then the prepared coatings were subjected to 15 h of heat treatment at 1073 K in a carbon and air environment to assess the impact of the atmosphere. The coating treated in a carbon atmosphere demonstrated more photocatalytic activity against methylene blue than air atmosphere coatings. This enhanced photocatalytic activity results from the findings that carbon-treated titania coatings have a nano-bump structure composed of titanium oxycarbide and rutile TiO_2. Moreover, it exhibited a smaller band gap energy of 1.48 eV than air-treated titania coatings (2.88 eV), which improves their good light absorption characteristics. It is depicted in Figure 12a–e [171].

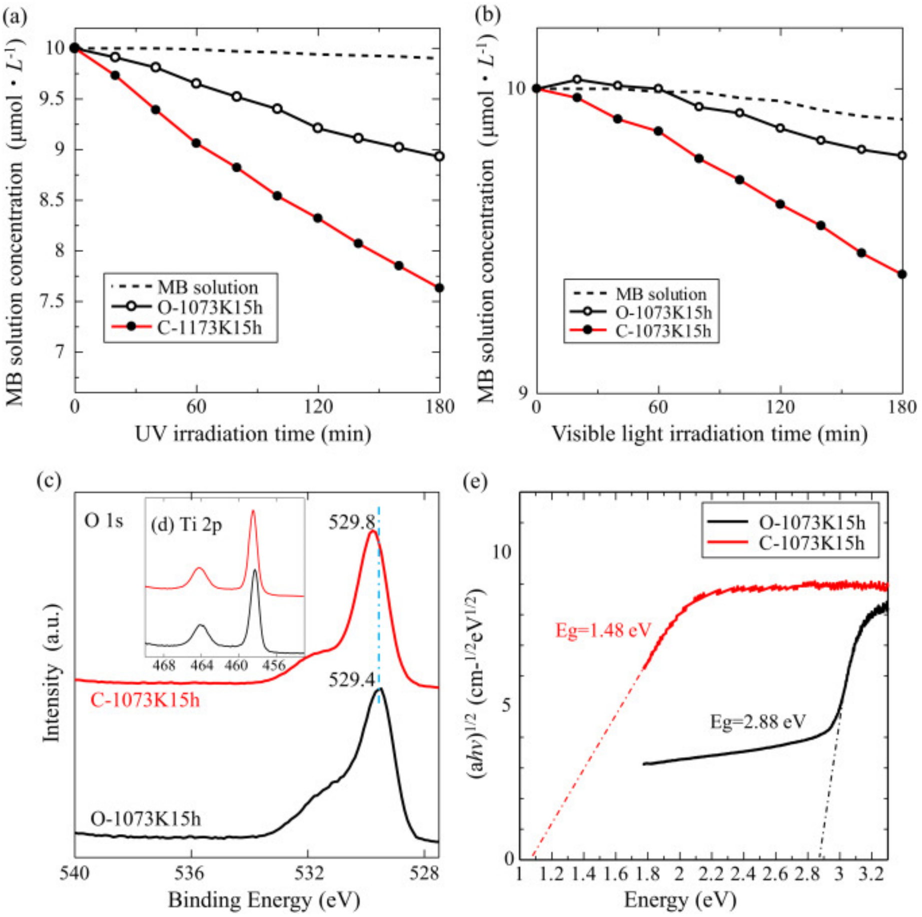

Figure 12. Photocatalytic behavior of TiC*x*O*y* coatings (prepared at carbon and air) over methylene blue degradation in the presence of (**a**) UV, and (**b**) Visible light; (**c**,**d**) XPS spectra for both TiC*x*O*y* coatings; (**e**) its band gap energies. Reproduced with permission [171], Copyright 2016, Elsevier.

Like titanium oxycarbide, silicon oxycarbide also possesses advantageous properties, including good oxidation stability and corrosion resistance. Eranezhuth Wasan Awin and colleagues attempted to incorporate titanium dioxide into silicon oxycarbide to create a TiO_2/SiOC composite with meso- and macroporous characteristics [172]. In addition to SiOC's advantageous properties, the incorporation of titanium oxide was anticipated to improve SiOC photocatalytic activity by boosting visible-light absorption and chemical stability. The surface morphology of the macroporous samples was found to be foamy, whereas mesoporous samples were found to be more agglomerated and have disordered structures. Moreover, the meso-/macroporous samples exhibited narrower band gap energy (2.05 eV and 2.75 eV, respectively) compared to pure titanium dioxide (2.9 eV), which enabled both composites to demonstrate promising photocatalytic degradation behavior over methylene blue dye under visible-light illumination.

According to our knowledge, oxy-carbides are utilized as a photocatalyst only in fewer papers. Even though oxycarbide compounds have intriguing properties, their synthesis processes are more complex than conventional photocatalysts. Therefore, it is necessary to create low-cost green synthetic methods with precise control over the anion stoichiometry to synthesize oxycarbide materials at a wide scale. This trend supports us in having a more profound knowledge of how to control the surface morphology of these materials and their creation, which helps to enhance their fundamental characteristics in the future.

6. Advantages of the Heteroanionic Photocatalyst

- ➢ Promising optical absorption property: Heteroanionic photocatalysts may absorb both visible and ultraviolet light effectively in order to drive an electron from VB to CB. Heteroanionic photocatalysts capture the visible portion of sunlight more efficiently than conventional photocatalysts [173,174].
- ➢ High diffusion rate: The electrons and holes in CB and VB of heteroanionic photocatalysts diffuse more rapidly from the bulk to the surface than traditional ones [175,176].
- ➢ Reasonable surface charge transfer property: Heteroanionic photocatalysts possess good surface charge transfer capability, interact well with various contaminants, and prolong charge-carrier recombination time [177,178].
- ➢ Effective oxygen utilization: Heteroanionic photocatalysts effectively utilize atmospheric oxygen as an oxidant; no additional oxidant is required [94,179].
- ➢ Utilize less UV Light: Heteroanionic materials utilize low-energy UV light to activate their photocatalytic properties [151].
- ➢ High stability: Heteroanionic photocatalysts are inexpensive, less toxic, stable, physiologically and chemically inert, largely insoluble, and recyclable [180].

7. Limitations of the Heteroanionic Photocatalyst

- ➢ Even though heteroanionic materials possess a narrower band than conventional photocatalysts, they still face quick recombination of the charge carriers during some catalytic reactions.
- ➢ Most heteroanionic materials employ expensive material (platinum) as a co-catalyst during hydrogen generation, which inevitably raises their synthesis costs.
- ➢ Current synthesis methods adopted for preparation for heteroanionic materials are very complex and do not possess precise control over the anion stoichiometry.
- ➢ Many heteroanionic materials are found to be potentially fit for photocatalysis, but they are utilized very rarely in catalytic reactions such as nitrogen fixation and CO_2 reduction compared to conventional catalysts.

8. Conclusions and Future Outlook

Energy harvesting from long-lasting sunlight has proven to be a promising answer to the world's energy needs and pollutant degradation. In the last few decades, most photocatalysts utilized for photocatalysis were basically made up of metal oxides/sulfides/nitrides. In recent days, heteroanionic photocatalysts that perform the same function with greater efficiency have accelerated research when compared with conventional catalysts. Heteroanionic photocatalysts were found to have a narrower band gap, which facilitates electron excitation when exposed to sunlight. In addition, these photocatalysts have a large surface area and small particle size, resulting in a low recombination rate. In this regard, we have emphasized the most recent developments of four types of heteroanionic photocatalysts, including oxynitride, oxysulfide, oxycarbide, and oxyhalide. Based on this review, we made a few recommendations and prospects to improve heteroanionic materials to advance photocatalysis technology further.

- ➢ **Simple and effective synthesis methods:** Although these materials have intriguing properties, most of their synthesis processes are more complex than conventional photocatalysts. Hence, it is necessary to create low-cost green synthetic methods to fabricate these photocatalysts on a wide scale at a high-efficiency level. For example, Xin-de tang et al. mainly adopted a simple approach to prepare a $La_3NbS_2O_5$ by varying its sulfurization time and synthesis temperatures [160]. It reduced preparation time to 1 h compared to the conventional synthesis process (which takes nine days).
- ➢ **Theoretical analysis**: Theoretical computations on the band gap and energy level of heteroanionic photocatalysts would provide theoretical guidance for building the desired structure and selecting suitable matching elements. For the fabrication of heteroanionic photocatalysts, a combination of experiment and computation approach is most required. Notably, DFT-based first-principles calculations can be employed to

investigate the characteristics of these materials and to gain a deeper understanding of the roles of the various components in the photocatalytic mechanism.

- **Developing new and cost-effective co-catalysts:** It is essential to fabricate novel and cost-effective co-catalysts that can effectively extract h^+/e^- from heteroanionic materials during catalytic reactions.
- **Doping and Heterostructures:** The photocatalytic efficiency of heteroanionic materials can be enhanced further through various approaches such as metal and non-metal doping, oxygen vacancies generation, sensitizers, carbonaceous materials, and heterostructures with other materials.
- **Defect control:** It was found that defects on the surface/bulk of heteroanionic materials will act as recombination sites for photogenerated charge carriers. Therefore, decreasing these defects is necessary, but it is very challenging due to the crucial heavy anionization process. Also, it is required to investigate new precursors and synthesis procedures under moderate conditions to eliminate defects in the heteroanionic materials. Hence, defect control will help to reduce the recombination sites resulting in an improvement in the efficiency of the heteroanionic materials.
- **Morphology control:** The morphology of these photocatalysts is the most determining parameter in light absorption capability, charge-carrier transport, and surface reaction rates. Hence, various nanotechnology approaches can be extensively used to control the morphology characteristics of heteroanionic materials. Reducing the particle size to the nanoscale reduces the migration distance, which makes more electron–hole pairs to travel onto the catalyst surface before recombination. A hierarchical structure will improve the water-splitting process of heteroanionic photocatalysts.

In conclusion, heteroanionic materials have greatly improved over the past decade due to extensive research and development efforts. Due to the synergetic effect of light harvesting, electron–hole separation and migration, and surface reaction during the photocatalysis activity, more future research needs to be focused on making materials with all characteristics. Constant efforts in this field are anticipated to result in photocatalysts capable of splitting water and degrading contaminants with high efficiency. In addition, the knowledge gained via investigating these compounds will illuminate the future creation of novel, efficient, and sustainable heteroanionic photocatalysts. For the advancement of the catalysis process, a unified set of assessment standards and parameters for the overall efficiency of photocatalysts, including their performance and stability, are necessary. It will help the research community reach its long-term, sustainable solar-fuel generation goal.

Author Contributions: Conceptualization, Y.S. and A.K.A.; methodology, Y.S. and A.K.A.; validation, Y.S., A.D. and L.A.O.; formal analysis, Y.S.; data curation Y.S., A.D. and L.A.O.; writing—original draft preparation, Y.S.; writing—review and editing, Y.S., M.R.S. and A.K.A.; supervision, M.R.S. and A.K.A. All authors have read and agreed to the published version of the manuscript.

Funding: This research was funded by FIC research grant, UBD/RSCH/1.3/FICBF(b)/2020/009.

Acknowledgments: The authors Y.S., A.D. and L.A.O. acknowledge the support from Universiti Brunei Darussalam through University Graduate Scholarship.

Conflicts of Interest: The authors declare no conflict of interest.

References

1. Roy, A.; Sharma, A.; Yadav, S.; Jule, L.T.; Krishnaraj, R. Nanomaterials for Remediation of Environmental Pollutants. *Bioinorg. Chem. Appl.* **2021**, *2021*, 1764647. [CrossRef] [PubMed]
2. Fang, B.; Xing, Z.; Sun, D.; Li, Z.; Zhou, W. Hollow semiconductor photocatalysts for solar energy conversion. *Adv. Powder Mater.* **2021**, *1*, 100021. [CrossRef]
3. Yan, T.; Yang, Q.; Feng, R.; Ren, X.; Zhao, Y.; Sun, M.; Yan, L.; Wei, Q. Highly effective visible-photocatalytic hydrogen evolution and simultaneous organic pollutant degradation over an urchin-like oxygen-doped $MoS_2/ZnIn_2S_4$ composite. *Front. Environ. Sci. Eng.* **2022**, *16*, 131. [CrossRef]

4. Subramanian, Y.; Mishra, B.; Mishra, R.P.; Kumar, N.; Bastia, S.; Anwar, S.; Gubendiran, R.; Chaudhary, Y.S. Efficient degradation of endocrine-disrupting compounds by heterostructured perovskite photocatalysts and its correlation with their ferroelectricity. *New J. Chem.* **2022**, *46*, 11851–11861. [CrossRef]
5. Subramanian, Y.; Mishra, B.; Mandal, S.; Gubendiran, R.; Chaudhary, Y.S. Design of heterostructured perovskites for enhanced photocatalytic activity: Insight into their charge carrier dynamics. *Mater. Today Proc.* **2020**, *35*, 179–185. [CrossRef]
6. Babel, S.; Sekartaji, P.A.; Sudrajat, H. ZnO nanoparticles for photodegradation of humic acid in water. *Environ. Sci. Pollut. Res.* **2021**, *28*, 31163–31173. [CrossRef]
7. Fujishima, A.; Honda, K. Electrochemical Photolysis of Water at a Semiconductor Electrode. *Nature* **1972**, *238*, 37–38. [CrossRef]
8. Kubiak, A.; Siwińska-Ciesielczyk, K.; Bielan, Z.; Zielińska-Jurek, A.; Jesionowski, T. Synthesis of highly crystalline photocatalysts based on TiO_2 and ZnO for the degradation of organic impurities under visible-light irradiation. *Adsorption* **2019**, *25*, 309–325. [CrossRef]
9. Etacheri, V.; Di Valentin, C.; Schneider, J.; Bahnemann, D.; Pillai, S.C. Visible-light activation of TiO_2 photocatalysts: Advances in theory and experiments. *J. Photochem. Photobiol. C Photochem. Rev.* **2015**, *25*, 1–29. [CrossRef]
10. Chaudhary, Y.S.; Woolerton, T.W.; Allen, C.S.; Warner, J.H.; Pierce, E.; Ragsdale, S.W.; Armstrong, F.A. Visible light-driven CO_2reduction by enzyme coupled CdS nanocrystals. *Chem. Commun.* **2011**, *48*, 58–60. [CrossRef]
11. Repo, E.; Rengaraj, S.; Pulkka, S.; Castangnoli, E.; Suihkonen, S.; Sopanen, M.; Sillanpää, M. Photocatalytic degradation of dyes by CdS microspheres under near UV and blue LED radiation. *Sep. Purif. Technol.* **2013**, *120*, 206–214. [CrossRef]
12. Singh, S.; Garg, S.; Saran, A.D. Photocatalytic activity of CdS and CdSe quantum dots for degradation of 3-aminopyridine. *Nanotechnol. Environ. Eng.* **2021**, *6*, 65. [CrossRef]
13. Toe, C.Y.; Scott, J.; Amal, R.; Ng, Y.H. Recent advances in suppressing the photocorrosion of cuprous oxide for photocatalytic and photoelectrochemical energy conversion. *J. Photochem. Photobiol. C Photochem. Rev.* **2018**, *40*, 191–211. [CrossRef]
14. Chatterjee, K.; Skrabalak, S.E. Durable Metal Heteroanionic Photocatalysts. *ACS Appl. Mater. Interfaces* **2021**, *13*, 36670–36678. [CrossRef]
15. Yaghoubi-Berijani, M.; Bahramian, B. Synthesis, and New Design into Enhanced Photocatalytic Activity of Porphyrin Immobilization on the Surface of Bismuth Oxyhalides Modified with Polyaniline. *J. Inorg. Organomet. Polym. Mater.* **2020**, *30*, 4637–4654. [CrossRef]
16. Wang, Q.; Nakabayashi, M.; Hisatomi, T.; Sun, S.; Akiyama, S.; Wang, Z.; Pan, Z.; Xiao, X.; Watanabe, T.; Yamada, T.; et al. Oxysulfide photocatalyst for visible-light-driven overall water splitting. *Nat. Mater.* **2019**, *18*, 827–832. [CrossRef]
17. Takata, T.; Pan, C.; Domen, K. Recent progress in oxynitride photocatalysts for visible-light-driven water splitting. *Sci. Technol. Adv. Mater.* **2015**, *16*, 033506. [CrossRef]
18. Kageyama, H.; Hayashi, K.; Maeda, K.; Attfield, J.P.; Hiroi, Z.; Rondinelli, J.M.; Poeppelmeier, K.R. Expanding frontiers in materials chemistry and physics with multiple anions. *Nat. Commun.* **2018**, *9*, 772. [CrossRef]
19. Zhang, B.; Xiao, J.; Jiao, S.; Zhu, H. Thermodynamic and thermoelectric properties of titanium oxycarbide with metal vacancy. *Int. J. Miner. Met. Mater.* **2022**, *29*, 787–795. [CrossRef]
20. Cuan, J.; Zhou, Y.; Zhang, J.; Zhou, T.; Liang, G.; Li, S.; Yu, X.; Pang, W.K.; Guo, Z. Multiple Anionic Transition-Metal Oxycarbide for Better Lithium Storage and Facilitated Multielectron Reactions. *ACS Nano* **2019**, *13*, 11665–11675. [CrossRef]
21. Fu, J.; Skrabalak, S.E. Enhanced Photoactivity from Single-Crystalline $SrTaO_2$ N Nanoplates Synthesized by Topotactic Nitridation. *Angew. Chem. Int. Ed.* **2017**, *56*, 14169–14173. [CrossRef] [PubMed]
22. Kato, D.; Hongo, K.; Maezono, R.; Higashi, M.; Kunioku, H.; Yabuuchi, M.; Suzuki, H.; Okajima, H.; Zhong, C.; Nakano, K.; et al. Valence Band Engineering of Layered Bismuth Oxyhalides toward Stable Visible-Light Water Splitting: Madelung Site Potential Analysis. *J. Am. Chem. Soc.* **2017**, *139*, 18725–18731. [CrossRef] [PubMed]
23. Xiao, M.; Wang, S.; Thaweesak, S.; Luo, B.; Wang, L. Tantalum (Oxy)Nitride: Narrow Bandgap Photocatalysts for Solar Hydrogen Generation. *Engineering* **2017**, *3*, 365–378. [CrossRef]
24. Lv, X.; Lam, F.L.Y.; Hu, X. A Review on Bismuth Oxyhalide (BiOX, X = Cl, Br, I) Based Photocatalysts for Wastewater Remediation. *Front. Catal.* **2022**, *2*, 839072. [CrossRef]
25. Zhang, J.; Tian, B.; Wang, L.; Xing, M.; Lei, J. Mechanism of Photocatalysis. In *Photocatalysis*; Springer: Berlin/Heidelberg, Germany, 2018; Volume 11, pp. 1–15. [CrossRef]
26. Saravanan, R.; Gracia, F.; Stephen, A. Basic Principles, Mechanism, and Challenges of Photocatalysis. In *Nanocomposites for Visible Light-Induced Photocatalysis*; Springer: Berlin/Heidelberg, Germany, 2017; pp. 19–40. [CrossRef]
27. Schneider, J.; Matsuoka, M.; Takeuchi, M.; Zhang, J.; Horiuchi, Y.; Anpo, M.; Bahnemann, D.W. Understanding TiO_2 Photocatalysis: Mechanisms and Materials. *Chem. Rev.* **2014**, *114*, 9919–9986. [CrossRef]
28. Guo, S.; Li, X.; Li, J.; Wei, B. Boosting photocatalytic hydrogen production from water by photothermally induced biphase systems. *Nat. Commun.* **2021**, *12*, 1343. [CrossRef]
29. Rodenberg, A.; Orazietti, M.; Probst, B.; Bachmann, C.; Alberto, R.; Baldridge, K.K.; Hamm, P. Mechanism of Photocatalytic Hydrogen Generation by a Polypyridyl-Based Cobalt Catalyst in Aqueous Solution. *Inorg. Chem.* **2014**, *54*, 646–657. [CrossRef]
30. Reza, M.S.; Ahmad, N.B.H.; Afroze, S.; Taweekun, J.; Sharifpur, M.; Azad, A.K. Hydrogen Production from Water Splitting through Photocatalytic Activity of Carbon-Based Materials. *Chem. Eng. Technol.* **2022**, 0930-7516. [CrossRef]

31. Subramanian, Y.; Ramasamy, V.; Karthikeyan, R.; Srinivasan, G.R.; Arulmozhi, D.; Gubendiran, R.K.; Sriramalu, M. Investigations on the enhanced dye degradation activity of heterogeneous $BiFeO_3$–$GdFeO_3$ nanocomposite photocatalyst. *Heliyon* **2019**, *5*, e01831. [CrossRef]
32. Subramanian, Y.; Ramasamy, V.; Gubendiran, R.K.; Srinivasan, G.R.; Arulmozhi, D. Structural, Optical, Thermal and Photocatalytic Dye Degradation Properties of $BiFeO_3$–WO_3 Nanocomposites. *J. Electron. Mater.* **2018**, *47*, 7212–7223. [CrossRef]
33. Serpone, N.; Emeline, A.V. Semiconductor Photocatalysis—Past, Present, and Future Outlook. *J. Phys. Chem. Lett.* **2012**, *3*, 673–677. [CrossRef]
34. Belver, C.; Bedia, J.; Gómez-Avilés, A.; Peñas-Garzón, M.; Rodriguez, J.J. Semiconductor Photocatalysis for Water Purification. In *Nanoscale Materials in Water Purification*; Elsevier: Amsterdam, The Netherlands, 2019; pp. 581–651. [CrossRef]
35. Zhang, L.; Ran, J.; Qiao, S.-Z.; Jaroniec, M. Characterization of semiconductor photocatalysts. *Chem. Soc. Rev.* **2019**, *48*, 5184–5206. [CrossRef]
36. Acar, C.; Dincer, I.; Naterer, G. Review of photocatalytic water-splitting methods for sustainable hydrogen production. *Int. J. Energy Res.* **2016**, *40*, 1449–1473. [CrossRef]
37. Zhang, F.; Wang, X.; Liu, H.; Liu, C.; Wan, Y.; Long, Y.; Cai, Z. Recent Advances and Applications of Semiconductor Photocatalytic Technology. *Appl. Sci.* **2019**, *9*, 2489. [CrossRef]
38. Li, Z.; Li, K.; Du, P.; Mehmandoust, M.; Karimi, F.; Erk, N. Carbon-based photocatalysts for hydrogen production: A review. *Chemosphere* **2022**, *308*, 135998. [CrossRef]
39. Xie, W.; Liu, L.; Cui, W.; An, W. Enhancement of Photocatalytic Activity under Visible Light Irradiation via the AgI@TCNQ Core-Shell Structure. *Materials* **2019**, *12*, 1679. [CrossRef]
40. Soni, V.; Khosla, A.; Singh, P.; Nguyen, V.-H.; Van Le, Q.; Selvasembian, R.; Hussain, C.M.; Thakur, S.; Raizada, P. Current perspective in metal oxide based photocatalysts for virus disinfection: A review. *J. Environ. Manag.* **2022**, *308*, 114617. [CrossRef]
41. Jia, L.; Tan, X.; Yu, T.; Ye, J. Mixed Metal Sulfides for the Application of Photocatalytic Energy Conversion. *Energy Fuels* **2022**, *36*, 11308–11322. [CrossRef]
42. Riente, P.; Noël, T. Application of metal oxide semiconductors in light-driven organic transformations. *Catal. Sci. Technol.* **2019**, *9*, 5186–5232. [CrossRef]
43. Ogawa, K.; Suzuki, H.; Zhong, C.; Sakamoto, R.; Tomita, O.; Saeki, A.; Kageyama, H.; Abe, R. Layered Perovskite Oxyiodide with Narrow Band Gap and Long Lifetime Carriers for Water Splitting Photocatalysis. *J. Am. Chem. Soc.* **2021**, *143*, 8446–8453. [CrossRef]
44. Wang, W.; Li, N.; Chi, Y.; Li, Y.; Yan, W.; Li, X.; Shao, C. Electrospinning of magnetical bismuth ferrite nanofibers with photocatalytic activity. *Ceram. Int.* **2012**, *39*, 3511–3518. [CrossRef]
45. Zhang, S.; Ou, X.; Xiang, Q.; Carabineiro, S.A.; Fan, J.; Lv, K. Research progress in metal sulfides for photocatalysis: From activity to stability. *Chemosphere* **2022**, *303*, 135085. [CrossRef] [PubMed]
46. Chandrasekaran, S.; Yao, L.; Deng, L.; Bowen, C.; Zhang, Y.; Chen, S.; Lin, Z.; Peng, F.; Zhang, P. Recent advances in metal sulfides: From controlled fabrication to electrocatalytic, photocatalytic and photoelectrochemical water splitting and beyond. *Chem. Soc. Rev.* **2019**, *48*, 4178–4280. [CrossRef] [PubMed]
47. Zhang, K.; Guo, L. Metal sulphide semiconductors for photocatalytic hydrogen production. *Catal. Sci. Technol.* **2013**, *3*, 1672–1690. [CrossRef]
48. Mehtab, A.; Ahmed, J.; Alshehri, S.M.; Mao, Y.; Ahmad, T. Rare earth doped metal oxide nanoparticles for photocatalysis: A perspective. *Nanotechnology* **2021**, *33*, 142001. [CrossRef]
49. Dong, S.; Feng, J.; Fan, M.; Pi, Y.; Hu, L.; Han, X.; Liu, M.; Sun, J.; Sun, J. Recent developments in heterogeneous photocatalytic water treatment using visible light-responsive photocatalysts: A review. *RSC Adv.* **2015**, *5*, 14610–14630. [CrossRef]
50. Zhang, J.; Gondal, M.; Wei, W.; Zhang, T.; Xu, Q.; Shen, K. Preparation of room temperature ferromagnetic $BiFeO_3$ and its application as an highly efficient magnetic separable adsorbent for removal of Rhodamine B from aqueous solution. *J. Alloys Compd.* **2012**, *530*, 107–110. [CrossRef]
51. Fan, T.; Chen, C.; Tang, Z. Hydrothermal synthesis of novel $BiFeO_3/BiVO_4$ heterojunctions with enhanced photocatalytic activities under visible light irradiation. *RSC Adv.* **2016**, *6*, 9994–10000. [CrossRef]
52. Gao, X.; Meng, X. Photocatalysis for Heavy Metal Treatment: A Review. *Processes* **2021**, *9*, 1729. [CrossRef]
53. Cho, C.M.; Noh, J.H.; Cho, I.-S.; An, J.-S.; Hong, K.S.; Kim, J.Y. Low-Temperature Hydrothermal Synthesis of Pure $BiFeO_3$Nanopowders Using Triethanolamine and Their Applications as Visible-Light Photocatalysts. *J. Am. Ceram. Soc.* **2008**, *91*, 3753–3755. [CrossRef]
54. Martins, P.M.; Gomez, V.; Lopes, A.C.; Tavares, C.J.; Botelho, G.; Irusta, S.; Lanceros-Mendez, S. Improving Photocatalytic Performance and Recyclability by Development of Er-Doped and Er/Pr-Codoped TiO_2/Poly(vinylidene difluoride)–Trifluoroethylene Composite Membranes. *J. Phys. Chem. C* **2014**, *118*, 27944–27953. [CrossRef]
55. Kuriki, R.; Ichibha, T.; Hongo, K.; Lu, D.; Maezono, R.; Kageyama, H.; Ishitani, O.; Oka, K.; Maeda, K. A Stable, Narrow-Gap Oxyfluoride Photocatalyst for Visible-Light Hydrogen Evolution and Carbon Dioxide Reduction. *J. Am. Chem. Soc.* **2018**, *140*, 6648–6655. [CrossRef]
56. Ogawa, K.; Nakada, A.; Suzuki, H.; Tomita, O.; Higashi, M.; Saeki, A.; Kageyama, H.; Abe, R. Flux Synthesis of Layered Oxyhalide Bi_4NbO_8Cl Photocatalyst for Efficient Z-Scheme Water Splitting Under Visible Light. *ACS Appl. Mater. Interfaces* **2018**, *11*, 5642–5650. [CrossRef]

57. Edalati, P.; Shen, X.-F.; Watanabe, M.; Ishihara, T.; Arita, M.; Fuji, M.; Edalati, K. High-entropy oxynitride as a low-bandgap and stable photocatalyst for hydrogen production. *J. Mater. Chem. A* **2021**, *9*, 15076–15086. [CrossRef]
58. Maeda, K.; Domen, K. Oxynitride materials for solar water splitting. *MRS Bull.* **2011**, *36*, 25–31. [CrossRef]
59. Vonrüti, N.; Aschauer, U. Band-gap engineering in AB(O_xS_{1-x})$_3$ perovskite oxysulfides: A route to strongly polar materials for photocatalytic water splitting. *J. Mater. Chem. A* **2019**, *7*, 15741–15748. [CrossRef]
60. Haman, Z.; Khossossi, N.; Kibbou, M.; Bouziani, I.; Singh, D.; Essaoudi, I.; Ainane, A.; Ahuja, R. Janus Aluminum Oxysulfide Al_2OS: A promising 2D direct semiconductor photocatalyst with strong visible light harvesting. *Appl. Surf. Sci.* **2022**, *589*, 152997. [CrossRef]
61. Fuertes, A. Synthetic approaches in oxynitride chemistry. *Prog. Solid State Chem.* **2018**, *51*, 63–70. [CrossRef]
62. Ahmed, M.; Xinxin, G. A review of metal oxynitrides for photocatalysis. *Inorg. Chem. Front.* **2016**, *3*, 578–590. [CrossRef]
63. Ebbinghaus, S.G.; Abicht, H.-P.; Dronskowski, R.; Müller, T.; Reller, A.; Weidenkaff, A. Perovskite-related oxynitrides—Recent developments in synthesis, characterisation and investigations of physical properties. *Prog. Solid State Chem.* **2009**, *37*, 173–205. [CrossRef]
64. Fuertes, A. Chemistry and applications of oxynitride perovskites. *J. Mater. Chem.* **2012**, *22*, 3293–3299. [CrossRef]
65. Moriya, Y.; Takata, T.; Domen, K. Recent progress in the development of (oxy)nitride photocatalysts for water splitting under visible-light irradiation. *Co-ord. Chem. Rev.* **2013**, *257*, 1957–1969. [CrossRef]
66. Fuertes, A. Metal oxynitrides as emerging materials with photocatalytic and electronic properties. *Mater. Horizons* **2015**, *2*, 453–461. [CrossRef]
67. Abeysinghe, D.; Skrabalak, S.E. Toward Shape-Controlled Metal Oxynitride and Nitride Particles for Solar Energy Applications. *ACS Energy Lett.* **2018**, *3*, 1331–1344. [CrossRef]
68. Miyoshi, A.; Maeda, K. Recent Progress in Mixed-Anion Materials for Solar Fuel Production. *Sol. RRL* **2020**, *5*, 2000521. [CrossRef]
69. Higashi, M.; Abe, R.; Ishikawa, A.; Takata, T.; Ohtani, B.; Domen, K. Z-scheme Overall Water Splitting on Modified-TaON Photocatalysts under Visible Light ($\lambda < 500$ nm). *Chem. Lett.* **2008**, *37*, 138–139. [CrossRef]
70. Maeda, K.; Domen, K. New Non-Oxide Photocatalysts Designed for Overall Water Splitting under Visible Light. *J. Phys. Chem. C* **2007**, *111*, 7851–7861. [CrossRef]
71. Chun, W.-J.; Ishikawa, A.; Fujisawa, H.; Takata, T.; Kondo, J.N.; Hara, M.; Kawai, M.; Matsumoto, A.Y.; Domen, K. Conduction and Valence Band Positions of Ta_2O_5, TaON, and Ta_3N_5 by UPS and Electrochemical Methods. *J. Phys. Chem. B* **2003**, *107*, 1798–1803. [CrossRef]
72. Zhang, P.; Zhang, J.; Gong, J. Tantalum-based semiconductors for solar water splitting. *Chem. Soc. Rev.* **2014**, *43*, 4395–4422. [CrossRef]
73. Tessier, F.; Marchand, R. Ternary and higher order rare-earth nitride materials: Synthesis and characterization of ionic-covalent oxynitride powders. *J. Solid State Chem.* **2003**, *171*, 143–151. [CrossRef]
74. Hellwig, A.; Hendry, A. Formation of barium-tantalum oxynitrides. *J. Mater. Sci.* **1994**, *29*, 4686–4693. [CrossRef]
75. Clarke, S.J.; Guinot, B.P.; Michie, C.W.; Calmont, M.J.C.; Rosseinsky, M.J. Oxynitride Perovskites: Synthesis and Structures of $LaZrO_2N$, $NdTiO_2N$, and $LaTiO_2N$ and Comparison with Oxide Perovskites. *Chem. Mater.* **2001**, *14*, 288–294. [CrossRef]
76. Yang, M.; Rodgers, J.A.; Middler, L.C.; Oró-Solé, J.; Jorge, A.B.; Fuertes, A.; Attfield, J.P. Direct Solid-State Synthesis at High Pressures of New Mixed-Metal Oxynitrides: $RZrO_2N$ (R = Pr, Nd, and Sm). *Inorg. Chem.* **2009**, *48*, 11498–11500. [CrossRef]
77. Kim, Y.-I.; Si, W.; Woodward, P.M.; Sutter, E.; Park, A.S.; Vogt, T. Epitaxial Thin-Film Deposition and Dielectric Properties of the Perovskite Oxynitride $BaTaO_2N$. *Chem. Mater.* **2007**, *19*, 618–623. [CrossRef]
78. Le Paven-Thivet, C.; Ishikawa, A.; Ziani, A.; Le Gendre, L.; Yoshida, M.; Kubota, J.; Tessier, F.; Domen, K. Photoelectrochemical Properties of Crystalline Perovskite Lanthanum Titanium Oxynitride Films under Visible Light. *J. Phys. Chem. C* **2009**, *113*, 6156–6162. [CrossRef]
79. Murphy, A.; Barnes, P.; Randeniya, L.; Plumb, I.; Grey, I.; Horne, M.; Glasscock, J.A. Efficiency of solar water splitting using semiconductor electrodes. *Int. J. Hydrogen Energy* **2006**, *31*, 1999–2017. [CrossRef]
80. Hara, M.; Hitoki, G.; Takata, T.; Kondo, J.N.; Kobayashi, H.; Domen, K. TaON and Ta_3N_5 as new visible light driven photocatalysts. *Catal. Today* **2003**, *78*, 555–560. [CrossRef]
81. Takata, T.; Pan, C.; Domen, K. Design and Development of Oxynitride Photocatalysts for Overall Water Splitting under Visible Light Irradiation. *Chemelectrochem* **2015**, *3*, 31–37. [CrossRef]
82. Hara, M.; Chiba, E.; Ishikawa, A.; Takata, T.; Kondo, A.J.N.; Domen, K. Ta_3N_5 and TaON Thin Films on Ta Foil: Surface Composition and Stability. *J. Phys. Chem. B* **2003**, *107*, 13441–13445. [CrossRef]
83. Maegli, A.E.; Otal, E.H.; Hisatomi, T.; Yoon, S.; Leroy, C.M.; Schäuble, N.; Lu, Y.; Grätzel, M.; Weidenkaff, A. Perovskite-Type $LaTiO_2N$ Oxynitrides for Solar Water Splitting: Influence of the Synthesis Conditions. *Energy Procedia* **2012**, *22*, 61–66. [CrossRef]
84. Rachel, A.; Ebbinghaus, S.; Güngerich, M.; Klar, P.; Hanss, J.; Weidenkaff, A.; Reller, A. Tantalum and niobium perovskite oxynitrides: Synthesis and analysis of the thermal behaviour. *Thermochim. Acta* **2005**, *438*, 134–143. [CrossRef]
85. Xu, J.; Pan, C.; Takata, T.; Domen, K. Photocatalytic overall water splitting on the perovskite-type transition metal oxynitride $CaTaO_2N$ under visible light irradiation. *Chem. Commun.* **2015**, *51*, 7191–7194. [CrossRef] [PubMed]
86. Hafez, A.M.; Zedan, A.F.; AlQaradawi, S.Y.; Salem, N.M.; Allam, N.K. Computational study on oxynitride perovskites for CO_2 photoreduction. *Energy Convers. Manag.* **2016**, *122*, 207–214. [CrossRef]

87. Matoba, T.; Maeda, K.; Domen, K. Activation of $BaTaO_2N$ Photocatalyst for Enhanced Non-Sacrificial Hydrogen Evolution from Water under Visible Light by Forming a Solid Solution with $BaZrO_3$. *Chem. A Eur. J.* **2011**, *17*, 14731–14735. [CrossRef] [PubMed]
88. Yamasita, D.; Takata, T.; Hara, M.; Kondo, J.N.; Domen, K. Recent progress of visible-light-driven heterogeneous photocatalysts for overall water splitting. *Solid State Ionics* **2004**, *172*, 591–595. [CrossRef]
89. Kasahara, A.; Nukumizu, K.; Hitoki, G.; Takata, T.; Kondo, J.N.; Hara, M.; Kobayashi, H.; Domen, K. Photoreactions on $LaTiO_2N$ under Visible Light Irradia-tion. *J. Phys. Chem. A* **2002**, *106*, 6750–6753. [CrossRef]
90. Wei, S.; Xu, X. Boosting photocatalytic water oxidation reactions over strontium tantalum oxynitride by structural laminations. *Appl. Catal. B Environ.* **2018**, *228*, 10–18. [CrossRef]
91. Siritanaratkul, B.; Maeda, K.; Hisatomi, T.; Domen, K. Synthesis and Photocatalytic Activity of Perovskite Niobium Oxynitrides with Wide Visible-Light Absorption Bands. *Chemsuschem* **2010**, *4*, 74–78. [CrossRef]
92. Hisatomi, T.; Katayama, C.; Teramura, K.; Takata, T.; Moriya, Y.; Minegishi, T.; Katayama, M.; Nishiyama, H.; Yamada, T.; Domen, K. The Effects of Preparation Conditions for a $BaNbO_2N$ Photocatalyst on Its Physical Properties. *ChemSusChem* **2014**, *7*, 2016–2021. [CrossRef]
93. Hisatomi, T.; Katayama, C.; Moriya, Y.; Minegishi, T.; Katayama, M.; Nishiyama, H.; Yamada, T.; Domen, K. Photocatalytic oxygen evolution using $BaNbO_2N$ modified with cobalt oxide under photoexcitation up to 740 nm. *Energy Environ. Sci.* **2013**, *6*, 3595–3599. [CrossRef]
94. Mohan, H.; Yoo, S.; Thimmarayan, S.; Oh, H.S.; Kim, G.; Seralathan, K.-K.; Shin, T. Nickel decorated manganese oxynitride over graphene nanosheets as highly efficient visible light driven photocatalysts for acetylsalicylic acid degradation. *Environ. Pollut.* **2021**, *289*, 117864. [CrossRef]
95. Hitoki, G.; Takata, T.; Kondo, J.N.; Hara, M.; Kobayashi, H.; Domen, K. (Oxy)nitrides as New Photocatalysts for Water Splitting under Visible Light Irradiation. *Electrochemistry* **2002**, *70*, 463–465. [CrossRef]
96. Hu, C.-C.; Teng, H. Gallium Oxynitride Photocatalysts Synthesized from $Ga(OH)_3$ for Water Splitting under Visible Light Irradiation. *J. Phys. Chem. C* **2010**, *114*, 20100–20106. [CrossRef]
97. Menon, S.S.; Hafeez, H.Y.; Gupta, B.; Baskar, K.; Bhalerao, G.; Hussain, S.; Neppolian, B.; Singh, S. ZnO:InN oxynitride: A novel and unconventional photocatalyst for efficient UV–visible light driven hydrogen evolution from water. *Renew. Energy* **2019**, *141*, 760–769. [CrossRef]
98. Cheng, H.; Huang, B.; Dai, Y. Engineering BiOX (X = Cl, Br, I) nanostructures for highly efficient photocatalytic applications. *Nanoscale* **2013**, *6*, 2009–2026. [CrossRef]
99. Gordon, M.N.; Chatterjee, K.; Lambright, A.L.; Bueno, S.L.A.; Skrabalak, S.E. Organohalide Precursors for the Continuous Production of Photocatalytic Bismuth Oxyhalide Nanoplates. *Inorg. Chem.* **2020**, *60*, 4218–4225. [CrossRef]
100. Huang, W.L.; Zhu, Q. Electronic structures of relaxed BiOX (X = F, Cl, Br, I) photocatalysts. *Comput. Mater. Sci.* **2008**, *43*, 1101–1108. [CrossRef]
101. Li, J.; Yu, Y.; Zhang, L. Bismuth oxyhalide nanomaterials: Layered structures meet photocatalysis. *Nanoscale* **2014**, *6*, 8473–8488. [CrossRef]
102. Li, J.; Zhang, L.; Li, Y.; Yu, Y. Synthesis and internal electric field dependent photoreactivity of Bi_3O_4Cl single-crystalline nanosheets with high {001} facet exposure percentages. *Nanoscale* **2013**, *6*, 167–171. [CrossRef]
103. Lou, Z.; Wang, P.; Huang, B.; Dai, Y.; Qin, X.; Zhang, X.; Wang, Z.; Liu, Y. Enhancing Charge Separation in Photocatalysts with Internal Polar Electric Fields. *Chemphotochem* **2017**, *1*, 136–147. [CrossRef]
104. Barhoumi, M.; Said, M. Correction of band-gap energy and dielectric function of BiOX bulk with GW and BSE. *Optik* **2020**, *216*, 164631. [CrossRef]
105. Li, M.; Huang, H.; Yu, S.; Tian, N.; Zhang, Y. Facet, Junction and Electric Field Engineering of Bismuth-Based Materials for Photocatalysis. *Chemcatchem* **2018**, *10*, 4477–4496. [CrossRef]
106. Sakthivel, T.; Venugopal, G.; Durairaj, A.; Vasanthkumar, S.; Huang, X. Utilization of the internal electric field in semiconductor photocatalysis: A short review. *J. Ind. Eng. Chem.* **2018**, *72*, 18–30. [CrossRef]
107. Yang, Y.; Zhang, C.; Lai, C.; Zeng, G.; Huang, D.; Cheng, M.; Wang, J.; Chen, F.; Zhou, C.; Xiong, W. BiOX (X = Cl, Br, I) photocatalytic nanomaterials: Applications for fuels and environmental management. *Adv. Colloid Interface Sci.* **2018**, *254*, 76–93. [CrossRef] [PubMed]
108. Ye, L.; Tian, L.; Peng, T.; Zan, L. Synthesis of highly symmetrical BiOI single-crystal nanosheets and their {001} facet-dependent photoactivity. *J. Mater. Chem.* **2011**, *21*, 12479–12484. [CrossRef]
109. Tu, X.; Luo, S.; Chen, G.; Li, J. One-Pot Synthesis, Characterization, and Enhanced Photocatalytic Activity of a BiOBr-Graphene Composite. *Chem. A Eur. J.* **2012**, *18*, 14359–14366. [CrossRef]
110. Zhang, K.; Zhang, D.; Liu, J.; Ren, K.; Luo, H.; Peng, Y.; Li, G.; Yu, X. A novel nanoreactor framework of iodine-incorporated BiOCl core–shell structure: Enhanced light-harvesting system for photocatalysis. *CrystEngComm* **2011**, *14*, 700–707. [CrossRef]
111. Zhang, W.; Zhang, Q.; Dong, F. Visible-Light Photocatalytic Removal of NO in Air over BiOX (X = Cl, Br, I) Single-Crystal Nanoplates Prepared at Room Temperature. *Ind. Eng. Chem. Res.* **2013**, *52*, 6740–6746. [CrossRef]
112. Ma, Z.; Li, P.; Ye, L.; Zhou, Y.; Su, F.; Ding, C.; Xie, H.; Bai, Y.; Wong, P.K. Oxygen vacancies induced exciton dissociation of flexible BiOCl nanosheets for effective photocatalytic CO_2 conversion. *J. Mater. Chem. A* **2017**, *5*, 24995–25004. [CrossRef]
113. Kong, X.Y.; Lee, W.P.C.; Ong, W.-J.; Chai, S.-P.; Mohamed, A.R. Oxygen-Deficient BiOBr as a Highly Stable Photocatalyst for Efficient CO_2Reduction into Renewable Carbon-Neutral Fuels. *Chemcatchem* **2016**, *8*, 3074–3081. [CrossRef]

114. Li, K.-L.; Lee, W.W.; Lu, C.-S.; Dai, Y.-M.; Chou, S.-Y.; Chen, H.-L.; Lin, H.-P.; Chen, C.-C. Synthesis of BiOBr, Bi_3O_4Br, and $Bi_{12}O_{17}Br_2$ by controlled hydrothermal method and their photocatalytic properties. *J. Taiwan Inst. Chem. Eng.* **2014**, *45*, 2688–2697. [CrossRef]
115. Xiao, X.; Zhang, W.-D. Facile synthesis of nanostructured BiOI microspheres with high visible light-induced photocatalytic activity. *J. Mater. Chem.* **2010**, *20*, 5866–5870. [CrossRef]
116. Xiong, J.; Cheng, G.; Li, G.; Qin, F.; Chen, R. Well-crystallized square-like 2D BiOCl nanoplates: Mannitol-assisted hydrothermal synthesis and improved visible-light-driven photocatalytic performance. *RSC Adv.* **2011**, *1*, 1542–1553. [CrossRef]
117. Cheng, H.; Huang, Y.; Wu, J.; Ling, Y.; Dong, L.; Zha, J.; Yu, M.; Zhu, Z. Controllable design of bismuth oxyiodides by in-situ self-template phase transformation and heterostructure construction for photocatalytic removal of gas-phase mercury. *Mater. Res. Bull.* **2020**, *131*, 110968. [CrossRef]
118. Lu, L.; Kong, L.; Jiang, Z.; Lai, H.H.-C.; Xiao, T.; Edwards, P.P. Visible-Light-Driven Photodegradation of Rhodamine B on Ag-Modified BiOBr. *Catal. Lett.* **2012**, *142*, 771–778. [CrossRef]
119. Li, G.; Qin, F.; Yang, H.; Lu, Z.; Sun, H.; Chen, R. Facile Microwave Synthesis of 3D Flowerlike BiOBr Nanostructures and Their Excellent Cr^{VI} Removal Capacity. *Eur. J. Inorg. Chem.* **2012**, *2012*, 2508–2513. [CrossRef]
120. Henle, J.; Simon, P.; Frenzel, A.; Scholz, S.; Kaskel, S. Nanosized BiOX (X = Cl, Br, I) Particles Synthesized in Reverse Microemulsions. *Chem. Mater.* **2007**, *19*, 366–373. [CrossRef]
121. Sharma, I.; Tripathi, G.K.; Sharma, V.K.; Tripathi, S.N.; Kurchania, R.; Kant, C.; Sharma, A.K.; Saini, K. One-pot synthesis of three bismuth oxyhalides (BiOCl, BiOBr, BiOI) and their photocatalytic properties in three different exposure conditions. *Cogent Chem.* **2015**, *1*, 1076371. [CrossRef]
122. Cui, P.; Wang, J.; Wang, Z.; Chen, J.; Xing, X.; Wang, L.; Yu, R. Bismuth oxychloride hollow microspheres with high visible light photocatalytic activity. *Nano Res.* **2016**, *9*, 593–601. [CrossRef]
123. Gao, P.; Yang, Y.; Yin, Z.; Kang, F.; Fan, W.; Sheng, J.; Feng, L.; Liu, Y.; Du, Z.; Zhang, L. A critical review on bismuth oxyhalide based photocatalysis for pharmaceutical active compounds degradation: Modifications, reactive sites, and challenges. *J. Hazard. Mater.* **2021**, *412*, 125186. [CrossRef]
124. Yu, H.; Han, Q. Effect of reaction mediums on photocatalytic performance of BiOX (X = Cl, Br, I). *Opt. Mater.* **2021**, *119*, 111399. [CrossRef]
125. Cui, J.; Tao, S.; Yang, X.; Yu, X.; Sun, S.; Yang, Q.; Wei, W.; Liang, S. Facile construction of nickel-doped hierarchical BiOCl architectures for enhanced visible-light-driven photocatalytic activities. *Mater. Res. Bull.* **2021**, *138*, 111208. [CrossRef]
126. Xia, J.; Di, J.; Li, H.; Xu, H.; Li, H.; Guo, S. Ionic liquid-induced strategy for carbon quantum dots/BiOX (X = Br, Cl) hybrid nanosheets with superior visible light-driven photocatalysis. *Appl. Catal. B Environ.* **2015**, *181*, 260–269. [CrossRef]
127. Xie, X.; Liu, Y.; Dong, X.; Lin, C.; Wen, X.; Yan, Q. Synthesis and characterization of Fe3O4/BiOI n-p heterojunction magnetic photocatalysts. *Appl. Surf. Sci.* **2018**, *455*, 742–747. [CrossRef]
128. Choi, Y.I.; Jeon, K.H.; Kim, H.S.; Lee, J.H.; Park, S.J.; Roh, J.E.; Khan, M.M.; Sohn, Y. TiO2/BiOX (X=Cl, Br, I) hybrid microspheres for artificial waste water and real sample treatment under visible light irradiation. *Sep. Purif. Technol.* **2016**, *160*, 28–42. [CrossRef]
129. Li, J.; Lu, T.; Zhao, Z.; Xu, R.; Li, Y.; Huang, Y.; Yang, C.; Zhang, S.; Tang, Y. Preparation of heterostructured ternary Cd/CdS/BiOCl photocatalysts for enhanced visible-light photocatalytic degradation of organic pollutants in wastewater. *Inorg. Chem. Commun.* **2020**, *121*, 108236. [CrossRef]
130. Adenuga, D.O.; Tichapondwa, S.M.; Chirwa, E.M. Facile synthesis of a Ag/AgCl/BiOCl composite photocatalyst for visible–light-driven pollutant removal. *J. Photochem. Photobiol. A Chem.* **2020**, *401*, 112747. [CrossRef]
131. Lee, G.-J.; Zheng, Y.-C.; Wu, J.J. Fabrication of hierarchical bismuth oxyhalides (BiOX, X = Cl, Br, I) materials and application of photocatalytic hydrogen production from water splitting. *Catal. Today* **2018**, *307*, 197–204. [CrossRef]
132. Wei, Z.; Liu, J.; Fang, W.; Qin, Z.; Jiang, Z.; Shangguan, W. A visible-light driven novel layered perovskite oxyhalide Bi_4MO_8X (M = Nb, Ta; X = Cl, Br) constructed using BiOX (X = Cl, Br) for enhanced photocatalytic hydrogen evolution. *Catal. Sci. Technol.* **2018**, *8*, 3774–3784. [CrossRef]
133. Ye, L.; Jin, X.; Liu, C.; Ding, C.; Xie, H.; Chu, K.H.; Wong, P.K. Thickness-ultrathin and bismuth-rich strategies for BiOBr to enhance photoreduction of CO_2 into solar fuels. *Appl. Catal. B Environ.* **2016**, *187*, 281–290. [CrossRef]
134. Bai, Y.; Yang, P.; Wang, P.; Xie, H.; Dang, H.; Ye, L. Semimetal bismuth mediated UV–vis-IR driven photo-thermocatalysis of $Bi_4O_5I_2$ for carbon dioxide to chemical energy. *J. CO2 Util.* **2018**, *23*, 51–60. [CrossRef]
135. Li, H.; Shang, J.; Ai, Z.; Zhang, L. Efficient Visible Light Nitrogen Fixation with BiOBr Nanosheets of Oxygen Vacancies on the Exposed {001} Facets. *J. Am. Chem. Soc.* **2015**, *137*, 6393–6399. [CrossRef]
136. Li, P.; Zhou, Z.; Wang, Q.; Guo, M.; Chen, S.; Low, J.; Long, R.; Liu, W.; Ding, P.; Wu, Y.; et al. Visible-Light-Driven Nitrogen Fixation Catalyzed by Bi_5O_7Br Nanostructures: Enhanced Performance by Oxygen Vacancies. *J. Am. Chem. Soc.* **2020**, *142*, 12430–12439. [CrossRef]
137. Lan, M.; Zheng, N.; Dong, X.; Hua, C.; Ma, H.; Zhang, X. Bismuth-rich bismuth oxyiodide microspheres with abundant oxygen vacancies as an efficient photocatalyst for nitrogen fixation. *Dalton Trans.* **2020**, *49*, 9123–9129. [CrossRef]
138. Wang, Q.; Hui, J.; Huang, Y.; Ding, Y.; Cai, Y.; Yin, S.; Li, Z.; Su, B. The preparation of BiOCl photocatalyst and its performance of photodegradation on dyes. *Mater. Sci. Semicond. Process.* **2014**, *17*, 87–93. [CrossRef]
139. Sun, X.; Wu, J.; Li, Q.; Liu, Q.; Qi, Y.; You, L.; Ji, Z.; He, P.; Sheng, P.; Ren, J.; et al. Fabrication of BiOIO3 with induced oxygen vacancies for efficient separation of the electron-hole pairs. *Appl. Catal. B Environ.* **2017**, *218*, 80–90. [CrossRef]

140. Cheng, H.; Wu, J.; Liu, Q.; Qi, Y.; Gu, M.; Lin, Y.; Hu, B.; Zhao, X.; Xiao, Y.; Wu, J. Morphology-dependent photocatalytic activity of Bi_5O_7I: Different charge separation efficiencies caused by facet synergy and internal electric field. *Mater. Lett.* **2019**, *252*, 252–255. [CrossRef]
141. Hu, M.; Yan, A.; Wang, X.; Huang, F.; Cui, Q.; Li, F.; Huang, J. Hydrothermal method to prepare Ce-doped BiOBr nanoplates with enhanced carrier transfer and photocatalytic activity. *Mater. Res. Bull.* **2019**, *116*, 89–97. [CrossRef]
142. Di, J.; Chen, C.; Yang, S.-Z.; Chen, S.; Duan, M.; Xiong, J.; Zhu, C.; Long, R.; Hao, W.; Chi, Z.; et al. Isolated single atom cobalt in Bi_3O_4Br atomic layers to trigger efficient CO_2 photoreduction. *Nat. Commun.* **2019**, *10*, 2840. [CrossRef]
143. Cui, D.; Wang, L.; Xu, K.; Ren, L.; Wang, L.; Yu, Y.; Du, Y.; Hao, W. Band-gap engineering of BiOCl with oxygen vacancies for efficient photooxidation properties under visible-light irradiation. *J. Mater. Chem. A* **2017**, *6*, 2193–2199. [CrossRef]
144. Gao, X.; Gong, C.; Wang, X.; Zhu, W.; Luo, Y. Facile synthesis of cobalt doped BiOCl ultrathin nanosheets as superior photocatalyst for degradation of carbamazepine under visible light. *J. Solid State Chem.* **2021**, *298*, 122131. [CrossRef]
145. Huang, J.; Zheng, X.; Liu, Y.; Wang, F.; Li, D.; Liu, H.; Li, R.; Chen, T.; Lv, W.; Liu, G. Integration of oxygen vacancies into BiOI via a facile alkaline earth ion-doping strategy for the enhanced photocatalytic performance toward indometacin remediation. *J. Hazard. Mater.* **2021**, *412*, 125147. [CrossRef] [PubMed]
146. Di, J.; Xia, J.; Chisholm, M.F.; Zhong, J.; Chen, C.; Cao, X.; Dong, F.; Chi, Z.; Chen, H.; Weng, Y.; et al. Defect-Tailoring Mediated Electron–Hole Separation in Single-Unit-Cell Bi $_3$ O $_4$ Br Nanosheets for Boosting Photocatalytic Hydrogen Evolution and Nitrogen Fixation. *Adv. Mater.* **2019**, *31*, e1807576. [CrossRef]
147. Fang, W.; Mi, Y.; Yang, Y.; Jiang, Y.; Liu, Y.; Shangguan, W. Conduction band tuning by strengthening s-p hybridization of novel layered oxyhalide Bi_4SbO_8Cl for efficient visible-light photocatalytic water splitting. *Mater. Today Chem.* **2022**, *26*, 101175. [CrossRef]
148. Peng, H.; Wang, L.; Xu, J.; Jiang, S.; Xu, X.; Zhang, Q. Novel $Bi_4O_5I_2/Bi_4O_5I_2$ hybrids: Synthesis, characterization, performance test. *Mater. Lett.* **2019**, *256*, 126694. [CrossRef]
149. Ishikawa, A.; Takata, T.; Kondo, J.N.; Hara, M.; Kobayashi, A.H.; Domen, K. Oxysulfide $Sm_2Ti_2S_2O_5$ as a Stable Photocatalyst for Water Oxidation and Reduction under Visible Light Irradiation ($\lambda \leq 650$ nm). *J. Am. Chem. Soc.* **2002**, *124*, 13547–13553. [CrossRef]
150. Nishioka, S.; Kanazawa, T.; Shibata, K.; Tsujimoto, Y.; Loye, H.-C.Z.; Maeda, K. A zinc-based oxysulfide photocatalyst $SrZn_2S_2O$ capable of reducing and oxidizing water. *Dalton Trans.* **2019**, *48*, 15778–15781. [CrossRef]
151. Zhang, G.; Wang, X. Oxysulfide Semiconductors for Photocatalytic Overall Water Splitting with Visible Light. *Angew. Chem. Int. Ed.* **2019**, *58*, 15580–15582. [CrossRef]
152. Pitha, J.J.; Smith, A.L.; Ward, R. The Preparation of Lanthanum Oxysulfide and its Properties as a Base Material for Phos-phors Stimulated by Infrared1. *J. Am. Chem. Soc.* **1947**, *69*, 1870–1871. [CrossRef]
153. Zachariasen, W.H. Crystal chemical studies of the 5f-series of elements. VII. The crystal structure of Ce_2O_2S, La_2O_2S and Pu_2O_2S. *Acta Crystallogr.* **1949**, *2*, 60–62. [CrossRef]
154. Wolff, C.M.; Frischmann, P.D.; Schulze, M.; Bohn, B.J.; Wein, R.; Livadas, P.; Carlson, M.T.; Jäckel, F.; Feldmann, J.; Würthner, F.; et al. All-in-one visible-light-driven water splitting by combining nanoparticulate and molecular co-catalysts on CdS nanorods. *Nat. Energy* **2018**, *3*, 862–869. [CrossRef]
155. Ishikawa, A.; Takata, T.; Matsumura, T.; Kondo, J.N.; Hara, M.; Kobayashi, A.H.; Domen, K. Oxysulfides $Ln_2Ti_2S_2O_5$ as Stable Photocatalysts for Water Oxidation and Reduction under Visible-Light Irradiation. *J. Phys. Chem. B* **2004**, *108*, 2637–2642. [CrossRef]
156. Abdullah, H.; Gultom, N.S.; Kuo, D.-H. Indium oxysulfide nanosheet photocatalyst for the hexavalent chromium detoxification and hydrogen evolution reaction. *J. Mater. Sci.* **2017**, *52*, 6249–6264. [CrossRef]
157. Ma, G.; Suzuki, Y.; Singh, R.B.; Iwanaga, A.; Moriya, Y.; Minegishi, T.; Liu, J.; Hisatomi, T.; Nishiyama, H.; Katayama, M.; et al. Photoanodic and photocathodic behaviour of $La_5Ti_2CuS_5O_7$ electrodes in the water splitting reaction. *Chem. Sci.* **2015**, *6*, 4513–4518. [CrossRef]
158. Song, Z.; Hisatomi, T.; Chen, S.; Wang, Q.; Ma, G.; Li, S.; Zhu, X.; Sun, S.; Domen, K. Visible-Light-Driven Photocatalytic Z-Scheme Overall Water Splitting in La $_5$ Ti $_2$ AgS $_5$ O $_7$ -based Powder-Suspension System. *Chemsuschem* **2018**, *12*, 1906–1910. [CrossRef]
159. Ogisu, K.; Ishikawa, A.; Teramura, K.; Toda, K.; Hara, M.; Domen, K. Lanthanum–Indium Oxysulfide as a Visible Light Driven Photocatalyst for Water Splitting. *Chem. Lett.* **2007**, *36*, 854–855. [CrossRef]
160. Tang, X.-D.; Ye, H.-Q.; Hu, H.-X. Sulfurization synthesis and photocatalytic activity of oxysulfide $La_3NbS_2O_5$. *Trans. Nonferrous Met. Soc. China* **2013**, *23*, 2644–2649. [CrossRef]
161. Zhang, F.; Maeda, K.; Takata, T.; Domen, K. Modification of oxysulfides with two nanoparticulate cocatalysts to achieve enhanced hydrogen production from water with visible light. *Chem. Commun.* **2010**, *46*, 7313–7315. [CrossRef]
162. Suzuki, T.; Hisatomi, T.; Teramura, K.; Shimodaira, Y.; Kobayashi, H.; Domen, K. A titanium-based oxysulfide photocatalyst: La5Ti2MS5O7 (M = Ag, Cu) for water reduction and oxidation. *Phys. Chem. Chem. Phys.* **2012**, *14*, 15475–15481. [CrossRef]
163. Ogisu, K.; Ishikawa, A.; Shimodaira, Y.; Takata, T.; Kobayashi, H.; Domen, K. Electronic Band Structures and Photochemical Properties of La−Ga-based Oxysulfides. *J. Phys. Chem. C* **2008**, *112*, 11978–11984. [CrossRef]
164. Pacquette, A.L.; Hagiwara, H.; Ishihara, T.; Gewirth, A.A. Fabrication of an oxysulfide of bismuth Bi_2O_2S and its photocatalytic activity in a Bi_2O_2S/In_2O_3 composite. *J. Photochem. Photobiol. A Chem.* **2013**, *277*, 27–36. [CrossRef]

165. Lopes, D.; Daniel-Da-Silva, A.L.; Sarabando, A.R.; Arias-Serrano, B.I.; Rodríguez-Aguado, E.; Rodríguez-Castellón, E.; Trindade, T.; Frade, J.R.; Kovalevsky, A.V. Design of Multifunctional Titania-Based Photocatalysts by Controlled Redox Reactions. *Materials* **2020**, *13*, 758. [CrossRef] [PubMed]
166. Hayami, W.; Tang, S.; Chiu, T.-W.; Tang, J. Reduction in Work Functions of Transition-Metal Carbides and Oxycarbides upon Oxidation. *ACS Omega* **2021**, *6*, 14559–14565. [CrossRef] [PubMed]
167. He, C.; Zheng, C.; Dai, W.; Fujita, T.; Zhao, J.; Ma, S.; Li, X.; Wei, Y.; Yang, J.; Wei, Z. Purification and Phase Evolution Mechanism of Titanium Oxycarbide (TiC_xO_y) Produced by the Thermal Reduction of Ilmenite. *Minerals* **2021**, *11*, 104. [CrossRef]
168. Calvillo, L.; García, G.; Paduano, A.; Guillen-Villafuerte, O.; Valero-Vidal, C.; Vittadini, A.; Bellini, M.; Lavacchi, A.; Agnoli, S.; Martucci, A.; et al. Electrochemical Behavior of TiO_xCy as Catalyst Support for Direct Ethanol Fuel Cells at Intermediate Temperature: From Planar Systems to Powders. *ACS Appl. Mater. Interfaces* **2015**, *8*, 716–725. [CrossRef]
169. Antolini, E.; Gonzalez, E.R. Tungsten-based materials for fuel cell applications. *Appl. Catal. B Environ.* **2010**, *96*, 245–266. [CrossRef]
170. Huang, K.; Li, Y.; Xing, Y. Carbothermal synthesis of titanium oxycarbide as electrocatalyst support with high oxygen evolution reaction activity. *J. Mater. Res.* **2012**, *28*, 454–460. [CrossRef]
171. Guan, S.; Hao, L.; Yoshida, H.; Pan, F.; Asanuma, H.; Lu, Y. Enhanced photocatalytic activity of photocatalyst coatings by heat treatment in carbon atmosphere. *Mater. Lett.* **2016**, *167*, 43–46. [CrossRef]
172. Awin, E.W.; Lale, A.; Kumar, K.C.N.H.; Demirci, U.B.; Bernard, S.; Kumar, R. Novel Precursor-Derived Meso-/Macroporous TiO_2/SiOC Nanocomposites with Highly Stable Anatase Nanophase Providing Visible Light Photocatalytic Activity and Superior Adsorption of Organic Dyes. *Materials* **2018**, *11*, 362. [CrossRef]
173. Maeda, K.; Takata, T.; Domen, K. (Oxy)nitrides and Oxysulfides as Visible-Light-Driven Photocatalysts for Overall Water Splitting. In *Energy Efficiency and Renewable Energy Through Nanotechnology*; Springer: Berlin/Heidelberg, Germany, 2011; pp. 487–529. [CrossRef]
174. Castillo-Cabrera, G.X.; Espinoza-Montero, P.J.; Alulema-Pullupaxi, P.; Mora, J.R.; Villacís-García, M.H. Bismuth Oxyhalide-Based Materials (BiOX: X = Cl, Br, I) and Their Application in Photoelectrocatalytic Degradation of Organic Pollutants in Water: A Review. *Front. Chem.* **2022**, *10*, 900622. [CrossRef]
175. Suresh, R.; Rajendran, S.; Kumar, P.S.; Hoang, T.K.; Soto-Moscoso, M. Halides and oxyhalides-based photocatalysts for abatement of organic water contaminants—An overview. *Environ. Res.* **2022**, *212*, 113149. [CrossRef]
176. Nava-Núñez, M.Y.; Jimenez-Relinque, E.; la Cruz, A.M.-D.; Castellote, M. Photocatalytic NO_x Removal in Bismuth-Oxyhalide (BiOX, X = I, Cl) Cement-Based Materials Exposed to Outdoor Conditions. *Catalysts* **2022**, *12*, 982. [CrossRef]
177. Talreja, N.; Afreen, S.; Ashfaq, M.; Chauhan, D.; Mera, A.C.; Rodríguez, C.; Mangalaraja, R. Bimetal (Fe/Zn) doped BiOI photocatalyst: An effective photodegradation of tetracycline and bacteria. *Chemosphere* **2021**, *280*, 130803. [CrossRef]
178. Zhang, S.; Wang, D.; Song, L. A novel F-doped BiOCl photocatalyst with enhanced photocatalytic performance. *Mater. Chem. Phys.* **2016**, *173*, 298–308. [CrossRef]
179. Cosham, S.D.; Celorrio, V.; Kulak, A.N.; Hyett, G. Observation of visible light activated photocatalytic degradation of stearic acid on thin films of tantalum oxynitride synthesized by aerosol assisted chemical vapour deposition. *Dalton Trans.* **2019**, *48*, 10619–10627. [CrossRef]
180. Di, J.; Xia, J.; Li, H.; Guo, S.; Dai, S. Bismuth oxyhalide layered materials for energy and environmental applications. *Nano Energy* **2017**, *41*, 172–192. [CrossRef]